# NOISE-ENHANCED DIRECTED TRANSPORT OF COLD ATOMS

A Thesis Presented to the Department of Theoretical and Applied Physics African University of Science and Technology, Abuja In partial fulfillment of the requirements for the award

**MASTER OF SCIENCE DEGREE**

by

**ODEKE, BONAVENTURE ANDREW**

supervised by

**PROFESSOR ANATOLE KENFACK**

African University of Science and Technology
www.aust.edu.ng
P.M.B 681, Garki, Abuja F.C.T
Nigeria.

March, 2021

## CERTIFICATION

This is to certify that the thesis titled, "**NOISE-ENHANCED DIRECTED TRANSPORT OF COLD ATOMS,"** submitted to the school of postgraduate studies, African University of Science and Technology (AUST), Abuja, Nigeria

for the award of a Master's degree is a record of original research carried out by

Odeke, Bonaventure Andrew in the department of Theoretical and Applied Physics.

**NOISE-ENHANCED DIRECTED TRANSPORT OF COLD ATOMS**

By

Odeke, Bonaventure Andrew

A THESIS APPROVED BY THE DEPARTMENT OF THEORETICAL AND APPLIED PHYSICS

RECOMMENDED:

……..……...……

Supervisor: Professor Anatole Kenfack

……..…….

Head, Theoretical and Applied Physics

APPROVED:

……..……..

Chief Academic Officer: Professor C. E. Chidume

……

Date

## ABSTRACT

The possibility of enhancing directed transport for a driven quantum particle in the presence of noise is investigated. Specifically, we deal with cold atoms trapped in an asymmetric optical lattice potential (ratchet potential), with amplitude noise, which is periodically switched on/off. Such potential in the absence of noise is the recently engineered optical lattice of ratchet type. The dynamics of this system are governed by the Time-Dependent Schrodinger Equation (TDSE) with noise or so-called Stochastic TDSE. Much like in the case of the TDSE, the Stochastic TDSE is solved utilizing the FFT Split Operator Method subject to a certain number of realization of the noise. Our observables of interest here are the current, the energy, and the momentum distribution wave function of the particle. In the absence of noise, we have been able to retrieve existing results in the literature demonstrating interesting directed transport properties within the quantum resonance regime (QR). We also checked that the counter-intuitive current reversal that occurs here goes hand in hand with the full classical chaos observed by solving the associated classical map of the system. Switching on the noise and still within QR and for weak potential strengths, optimal currents emerged for given noise intensities. At the limit of the very high noise intensity, the current saturates. On the other hand, for a strong potential strength, the noise suppresses the current and in some cases even leads to current reversal. The effect should be readily observable in experiments.

## ACKNOWLEDGEMENTS

First of all, I want to thank God Almighty for making this work to see the light of the day.

My appreciation also goes to my supervisor, professor Kenfack whose idea birthed this work and who has guided me throughout the journey of doing this research. You made the work easier by your camaraderie. You did not just supervise this thesis; you were there at my beck and call. You never got tired of my questions.

Also, my gratitude goes to my classmates, Gyang, Tofunmi, Kabir, and Denis. You are wonderful. Starting the original version of my code together shows love and unity. You guys were always there when I needed you.

I will not forget to thank my friend Tofunmi, Joshua, and Kabir who helped me with running my codes when I had a power failure in my place.

I am grateful to all those not mentioned here. You are not forgotten. I appreciate you.

My endless gratitude goes to our sponsors who allowed us to have our master's degree in this great university. Your efforts of making us the best will not be in vain as we will put Africa at the forefront in scientific research.

And lastly, to my parents, my siblings, their moral support was something I could never find anywhere. I love you dearly.

This work is dedicated to my family

# TABLE OF CONTENTS

## LIST OF FIGURES

# CHAPTER ONE

# INTRODUCTION

In this chapter, we started with the history of the Brownian ratchet. From the early twentieth century, the Smoluchowski ratchet to the mid-twentieth century, the Brillouin Paradox, the Feynman explanation of the earlier Smoluchowski ratchet and pawl system. We highlighted the necessary conditions for the one-directional motion of a ratchet device when an unbiased thermal fluctuation is present. The major condition that cuts across the operating mechanism of the ratchet system is that there must be a way to bring the system out of equilibrium. It is the most important of the conditions. This is already explained in detail in this chapter. We went further to explain a fundamental model of ratchet device, that is, a method or mechanism of achieving this out-of-equilibrium condition. This method is called the flashing mechanism where the potential is periodically flashed on and off. We explained this flashing mechanism because it is the method used in our model. We pointed out that the effect of thermal fluctuations is very significant at the molecular and nano level. In a later sub-section, we looked at some general relevance of the Brownian ratchet: the molecular proteins which help in cellular activities and the contraction of muscles. We concluded this chapter by explaining briefly how to cool an atom and trap it at the bottom of some potential well using a combination or interference of standing laser waves.

## 1.1 Brownian Ratchet and the Second Law of Thermodynamics

Brownian ratchets are devices that do work from the rectification of some microscopic fluctuation. For a Brownian ratchet to perform its duty, three conditions must be met. Two of which are from the individual words that make up the phrase, "Brownian ratchet." The word, "Brownian," is from the zigzag motion of pollen grain in a fluid that was first studied by Robert Brown. This is a typification of a fluctuating environment and that is the first condition – there must be a fluctuating environment. The second word, "ratchet," brings out the requirement of the necessary asymmetry into the system. The third condition which is the most important of them all is that the system must be out of equilibrium. It is the most

important because a fluctuating environment and the necessary asymmetry alone cannot get us a directed transport if the system is in equilibrium. The second law of thermodynamics prevents such directed motion, and this is majorly the scope of this chapter.

The origin of Brownian ratchet dates back to a thought experiment by Smoluchowski – his ratchet and pawl thought experiment where he proposed that one can get a unidirectional motion from such a system. It was later popularized by Feynman in his lecture The Feynman Lectures on Physics, Vol. 1 (1962) [1], where he explained the limitation imposed by the second law of thermodynamics on such a system. And as a result of this limitation, the system will have a net (average) zero motion.

Another machine that has the same principle as the ratchet device is the electrical rectifier. It was studied by Brillouin in 1950 [2]. These two machines would violate the second law of thermodynamics if they can produce useful work from the rectification of thermal fluctuations just from one heat reservoir.

### 1.1.1 **The Second Law of Thermodynamics**

In line with other physics laws, many physical processes do not occur because of thermodynamics' second law. The second law gives the direction and feasibility of physical processes. For example, though the conservation of energy principle is obeyed by having water in a glass at room temperature to cool itself spontaneously to form ice by releasing energy to the environment., it does not and cannot happen because of the implication of the second law.

Though the second law of thermodynamics has variant ways to state it, its first formulation dates back to Sadi Carnot in 1824 [3], who limits the efficiency of any heat engine operating between two given temperatures. In this chapter, we are especially interested in the equivalent statement of the second law given by Lord Kelvin, which can be stated as

> *There is no thermodynamic transformation whose sole effect is to extract heat from a heat reservoir and to convert it entirely into useful work.*

A heat reservoir is a system so big that the exchange of heat does not change its temperature. A variant way to state the second law is using the concept of entropy.

*The entropy of an isolated system never decreases.*

From this theory, it is evident that the second law is not time-symmetric and hence shows a preferential direction of time.

### 1.1.2 Brillouin Paradox

A diode is an electronic component that allows current to flow in just one direction. Its use became very popular in the 1950s due to the large progress in the production of semiconductor diodes.

Because of the innate asymmetry exhibited by diodes, one may want to know if this property could rectify thermal fluctuations and also the implications of the second law of thermodynamics on such a system.

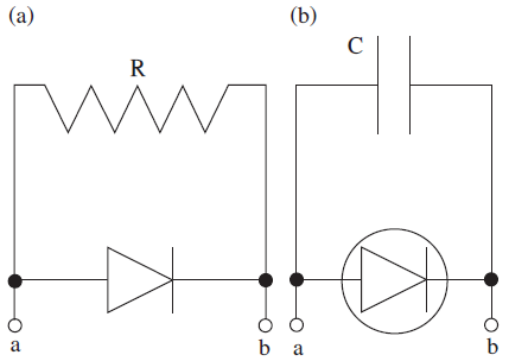


Fig. 1.1 (a) The Brillouin paradox, as initially formulated; is it possible for a diode to rectify the resistor's thermal fluctuations to have an output of a direct voltage, like a small battery? (b) The variant of the paradox initiated by Alkemade, where the resistor was substituted with a capacitor and a vacuum diode considered.

In 1950, Leon Brillouin, a French physicist explained how at thermal equilibrium, we can get thermal fluctuations rectified by a diode, thereby contradicting the second law of thermodynamics. This explanation is very intuitive but does not happen in reality. This is known as the Brillouin paradox. In Fig 1.1 (a), we have a simple circuit that is made up of a resistor and a diode. The voltage across the resistor

will be fluctuating due to the finite temperature and its associated thermal noise. The diode can rectify these fluctuations and we now have a direct voltage and hence a direct current which an electrical source of energy, able to do useful work. This makes perfect sense by intuition. But let's recall that this system is at equilibrium and as such limited by the second law of thermodynamics in operating in this manner. If we analyze this system accurately, we will see that we cannot have a direct current in such a circuit so that the system now agrees with the second law.

Rather than looking at the microscopic description of the original Brillouin paradox, we are going to look at a similar circuit that will help to bring out this explanation clearer. This circuit (a variant form of the Brillouin paradox circuit) was introduced by Alkemade and van Kampen and is shown in Fig 1.1 (b). In this figure, we have the resistor in the original Brillouin paradox replaced by a capacitor, and the diode by a vacuum diode. The logical inference is that if the intuitive explanation of the Brillouin paradox is true, then we should have an accumulation of charges on the plates of the capacitor. Let us see if this accumulation of charges on capacitor plates is possible.

Let us consider an initially uncharged capacitor. At some finite temperature, the capacitor will have some random charge as a result of its temperature. This type of random charge is called thermal noise. If a diode is not connected in the circuit, this random charge fluctuates between positive and negative values. The time averages of the associated voltage at any instant is $V_b - V_a = Q/C$, where $C$ is the capacitance. However, the average energy stored in the capacitor is not zero because it is computed as $\langle Q^2/2C \rangle = K_B T/2$ where $K_B$ is the Boltzmann constant and it is equal $1.38065\, x\, 10^{-23} J/K$. This is from the equipartition principle.

Though this average energy is small, one may think that by introducing a diode we will be able to harness it. That is, since the current fluctuates between positive and negative values, the diode should allow current in the direction it favours and blocks current in the direction it does not allow. As a result of this asymmetry of the diode, we would have some voltage offset that is greater than zero (i.e., $V_b - V_a > 0$)

which can do work. In this explanation, the system does useful work by operating solely at one temperature, thus contradicting the second law of thermodynamics. This should be surprising! In reality, we found out that the diode does not rectify this thermal noise. Why? For us to answer this question, we have to come down to the microscopic examination of the system.

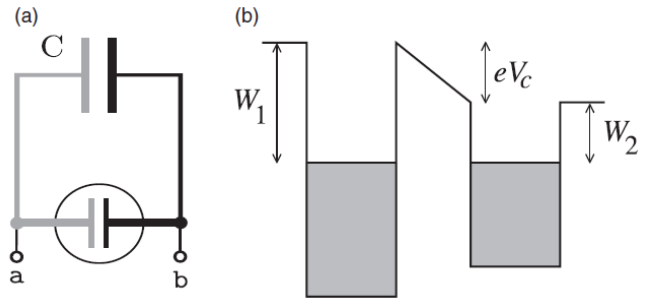


Fig 1.2 Alkemade diode: two metals with dissimilar work functions

Let us recall that the rectifier in our circuit is a vacuum diode [4], and its rectifying component is shown in Fig 1.2. The vacuum diode is made up of two electrodes with different work functions $W_1$ & $W_2$, both at equilibrium at temperature $T$, separated by a short distance, very small to allow the passage of electrons. The vacuum diode is connected to a capacitor. One assumption is that the diode's capacitance is negligible when compared to that of the capacitor.

To proceed to equilibrium electrons will have a net flux from the higher chemical potential (or Fermi level) to a lower one. At equilibrium, the chemical potential (Fermi level) of the two electrodes becomes equal. At this point, the net flow of electrons stops. That the electrons stop flowing from one electrode to the other does not mean that the potential in between them is zero, or that the potential difference across them is zero. There is a potential difference and an associated uniform electric field between these electrodes. This potential difference is a result of the different work functions of the two metals. We find that the uniform electric field allows the electron to move in a preferred direction (asymmetry) and that is

how the diode allows only flow of electron (current) in one direction preventing its flow in the opposite direction.

The work function of a metal is the minimum energy needed to remove an electron from that metal. As we said before, the potential difference is a result of the different work functions of the electrodes. It is given as $V_C = (W_1 - W_2)/e$, where $e = 1.60217657\, x\, 10^{-19}\, C$. The different work functions are shown clearly in Fig 1.2. Generally, for any two dissimilar materials, $V_C$ across them is referred to as *Contact potential*, and it is affected by two factors: the distance between the materials, and the presence of a surface contaminant. If both materials are metal, $V_C$ has a special name; it is called the *Volta potential*.

Let us assume that the right electrode initially has a higher Fermi level. As the system approaches equilibrium, we expect electrons to flow from this right electrode to the left, and then to the capacitor's plate in a clockwise direction charging up the capacitor to an equilibrium charge, $CV_C$, till the flux ceases. Since we said earlier that the capacitance of the diode is negligible when compared to that of the capacitor, then it implies that the charges on the diode's plate are also negligible. On the other hand, for a semiconductor diode, the contact potential is a result of the accumulation of opposite charges at the surface of the junction between the p and n-type semiconductor in the p-n junction diode. This region between the oppositely separated charges is called the depletion region. This same thing will happen in the vacuum diode (between the two plates of the electrodes if it is not connected to a capacitor).

Let us now look at the role played by thermal fluctuation for a system like this at equilibrium. First, the density probability for an energy fluctuation at temperature $T$ varies as $\exp(-E/K_BT)$. This is the Boltzmann factor. It means that at equilibrium for the Alkemade diode in Fig 1.2, the probability of electron to cross from the left electrode to the right electrode is equal to $\exp(-W_1/K_BT)$ since $W_1$ is the size of the barrier (minimum energy) to overcome. Also, the probability of electron to cross from right to left must be equal to $\exp(-(W_2 + eV_C)/K_BT)$ which is still equal to $\exp(-W_1/K_BT)$ since $W_2 + eV_C =$

$W_1$. Then there is an equal probability to either move from left to right or from right to left. There is a zero net flow of electrons from either of the electrodes and thus the diode does not rectify the thermal fluctuation as the Brillouin paradox suggested. This is in perfect agreement with the second law of thermodynamics as this law does not allow extraction of work from solely one temperature bath.

We have seen that at equilibrium and in the absence of an external bias voltage, the net flow of electrons in a diode is zero. There are situations when one can get a net flow of electrons. The first case is when there is an external voltage, $V$. This is the usual way to use a diode. Let say $V < V_C$, the barrier energy to be overcome by an electron moving from the left to right electrode will still be $W_1$ like in the case of no bias voltage. So the probability remains the same, $\exp(-W_1/K_BT)$. However, for electrons crossing from the right electrode to the left, the barrier width will be reduced by $-eV$ and the corresponding probability is $\exp(-(W_1 - eV)/K_BT)$, and thus an increased probability. Bringing both probabilities together, the net current/electron flow will be given by

$$I = A(exp(eV/K_BT) - 1) \quad (1.1)$$

Where A is a constant. The above equation (1.1) is the typical $I - V$ characteristics for most diodes. If $V$ is positive, the diode is said to be forward-biased and the current grows exponentially. If $V$ is negative, it is said to be reverse biased and the current saturates to a constant negative, though very little value. This negative constant current is called the *reverse saturation current* of a diode. The bias voltage ($V$ is positive) reduces or ($V$ is negative) increases the resistance associated with the contact potential. For $V$ is positive, the depletion layer gradually fizzles out and its formation is prevented as the external voltage is forced through the diode. Hence, the flow of current.

Another way the direct current is gotten is in the absence of a bias voltage but with the temperature of the two electrodes different, for instance, $T_1 < T_2$. This is fine because the system is no longer disobeying the second law of thermodynamics as it is no longer in equilibrium. Let us assume that each of the electrodes is at local equilibrium. The current in each direction should roughly vary as the corresponding equilibrium

probability of jumping over. As we considered the case where $T_2 > T_1$, the probability of crossing to the left $\exp(-W_1/K_B T_2)$ is greater than that of crossing to the left $\exp(-W_1/K_B T_1)$. Thus we expect a forward current. The diode in this scenario is acting as a small battery where thermal fluctuation through the temperature gradient is the energy power source. This phenomenon is called the thermoelectric effect or the Seeback effect since Seeback discovered it first in 1821 [5]. Today, this is the operating principle of a thermocouple – a viral temperature sensor.

Thus, from our analysis so far, we have seen from the Brillouin paradox how our intuition may not always be correct, clearly violating the second principle of thermodynamics. On the other hand, accurate microscopic examination leads to prediction in harmony with the second law. Let us now take a fresh look at the circuit of Fig 1.2 focusing on the *intuitive* approach which gave an incorrect prediction. But now, in a more detailed manner and at the microscopic level. Let us see if we can trace down the breaching of the second law of thermodynamics to some assumptions made via this approach.

A considerable defect of charge in the capacitor $\langle \tilde{Q} \rangle = CV_c - \langle Q \rangle$, will give a forward potential bias $V = \langle \tilde{Q} \rangle / C$. Therefore, from (1.1) we get an equation for the average charge at the capacitor,

$$\frac{d\tilde{Q}}{dt} = -A\left[exp\left(\frac{e\tilde{Q}}{CK_BT}\right) - 1\right] \tag{1.2}$$

Justifiable to illustrate the dynamics of the macroscopic fluctuation $\langle \tilde{Q} \rangle$ in situations that are not in equilibrium. One may be tempted to use this equation in modelling bare fluctuations, for instance, by seeing it as correct for $\tilde{Q}$ and adding a noise term $\xi(t)$,

$$\frac{d\tilde{Q}}{dt} = -A\left[exp\left(\frac{e\tilde{Q}}{CK_BT}\right) - 1\right] + \xi(t) \tag{1.3}$$

With $\langle \xi(t) \rangle = 0$. The fluctuations $\tilde{Q}$ is small and then we could expand the exponential in (1.3) to

$$\frac{d\tilde{Q}}{dt} = -A\left(\frac{e}{CK_BT}\tilde{Q} + \frac{e^2}{2(CK_BT)^2}\tilde{Q}^2\right) + \xi(t) \tag{1.4}$$

However, neither this above stochastic equation nor (1.3) admits the expected thermal equilibrium solution, with $\langle \tilde{Q} \rangle_{eq} = 0$ and $\langle \tilde{Q}^2 \rangle_{eq} = CK_BT$. This is clear by taking averages in (1.4). As a matter of choice, if nonzero values of $\langle \tilde{Q} \rangle_{eq}$ are used, (1.4) gives

$$\langle \tilde{Q} \rangle_{eq} = -\frac{1}{2}\frac{e}{CK_BT}\langle \tilde{Q}^2 \rangle_{eq} = -e/2 \tag{1.5}$$

a defect charge that would breach the second law. Such nonphysical result is nothing other than the Brillouin paradox, gotten through an inaccurate microscopic examination. The two equations (1.4) and (1.3) are not correct. It is not permissible to generalize a nonlinear equation that works for macroscopic quantities, like (1.2), to analyze fluctuating quantities at the microscopic level. This generally leads to inconsistencies, as already seen in the initial derivation. It is worth pointing out that it is the non-linearity of (1.2) that brings about the paradoxical results when its viability is stretched to accommodate microscopic fluctuations. When applied to microscopic fluctuations, the paradoxical results would not have been gotten if we had used the linearized version of (1.2). What I mean is that if the quadratic term in $\tilde{Q}$ appearing on the right-hand side of (1.4) is not considered, the equation would be correct, thus eliminating the seeming paradox.

### 1.1.3 Feynman Ratchet

In section 1.1.2, we looked at the electrical rectifier (the diode) and the Brillouin paradox. In this section, we are going to discuss the Feynman-Smoluchowski ratchet [6] which is just the mechanical analog of the diode.

Fig 1.3 is the mechanical rectifier. It is made up of a gear wheel on one side connected to an axle and a vane on the other side. On the gear wheel is the pawl which has a spring that bounces up and down as the gear wheel rotates. Because of the asymmetry of the gear wheel teeth, the pawl allows the gear wheel to move in only one direction, preventing it from moving in the opposite direction by gripping the teeth.

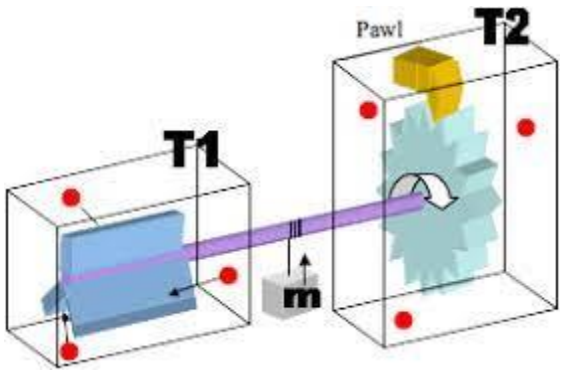


Fig 1.3. Smoluchowski and Feynman's ratchet and pawl system

The vane is immersed in a fluid at temperature $T_1$ so that the molecules or particles in the fluid are in Brownian motion and collide randomly with the vane. We assume that the system is very small so that the collision from the random moving particle can rotate the vane. Since there are random collisions on the vane, it will be able to move equally forward and backward direction. The pawl prevents the backward motion, and we get a net forward motion or rotation. Hence, it can be used to do work (to lift a body of mass, m against gravity). This is not possible as the ratchet does work at just one temperature. It contradicts the second law of thermodynamics just as the intuitive explanation of the Brillouin paradox of our electrical rectifier.

Feynman was able to explain that the machine can't convert the heat (of size proportional to $K_B T$) from the vane entirely to useful work if the system is at equilibrium. If the pawl is at the same temperature as the vane, thermal fluctuation will affect the spring attached to the pawl and damps its up and down motion so that it allows the teeth of the gear wheel to now move equally forward and backward, thereby resulting to no net motion in agreement with the second law of thermodynamics.

Let us say just like we have in Fig 1.3, that the ratchet wheel (specifically the pawl) is at a lower temperature $T_2$ (i.e., $T_2 < T_1$), then the system is no longer at equilibrium. In this case, we will have a net forward motion and the system can do useful work. The machine in this configuration works as a heat engine that absorbs heat from one heat reservoir (the vane), uses part of it to do work, and discards the

remaining into the cold reservoir (the pawl). Feynman did not only explain this concept clearly but also went ahead to calculate the efficiency of this machine in lifting a load of mass m. He used the formula for the efficiency of a Carnot engine operating quasi-statically, $\eta_C = 1 - T_2/T_1$. He underestimated $T_2$ thereby exaggerating the real efficiency, $\eta_C$.

Finally, the examination of the mechanical ratchet operating at just a single temperature results in some general considerations. In fact, it was structured to build a machine to get thermal fluctuation from just one heat reservoir. Energy fluctuations are room temperature, of the order of $K_B T = 4\ x\ 10^{-21}\ J$, which is very small from a macroscopic viewpoint. The energy of the pawl's spring or due to frictional force, or the gravitational energy of the weight are all generally in the macroscopic scale. Therefore, a mechanical ratchet of macroscopic size would not experience motion, not because of the second law, but as a result of the very small size of the thermal fluctuations. To observe the effect of these fluctuations, the ratchet would then need to be built at a smaller scale, the molecular scale, where these thermal fluctuations are not only appreciable but also play a major role. As we have discussed previously due to fluctuations, sometimes the ratchet would move in the forward direction and other times in the backward direction, and thus no net motion in agreement with the second law. But when compared with our macroscopic world, where such fluctuations are too little to be directly noticed, each time the wheels move seems like a temporary breach of the second law, underscoring the statistical nature of this law.

### 1.1.4 Equilibrium and Detailed Balance

Despite the analysis of sections 1.1.1 – 1.1.3, one may still want to understand what is in thermal equilibrium that usually cancels the spatial asymmetry of the system, hence putting a stop to the rectification of fluctuations. Lord Kelvin's formulation of the second law is somewhat axiomatic, and a general microscopic clarification of why there cannot be a rectification of thermal fluctuations for a system at thermal equilibrium is helpful.

In section 1.1.1 – 1.1.3, a physical explanation based on the Boltzmann factor in two simple systems was given. This type of analysis can however become more difficult to apply in more complex systems.

A general explanation can be given based on symmetry, detailed balance, which depends on the underlying reversibility of the molecular laws. Ludwig Boltzmann introduced Detailed balance in 1872 to prove the H-theorem, which explains the irreversibility tendency of the quantity H (supposed to be the entropy) to increase. It states that all processes at thermal equilibrium are equilibrated by their reverse processes.

The microscopic equations of motion are symmetric for inversion in time. Let us look at a system's trajectory if the velocities of all spots in the system at any specified instant were reversed, the system would go backward in time. At thermal equilibrium, the law of equal-a-priori probability says that a specified configuration and another with all velocities reversed are equally probable, inferring that any system's trajectory and its reversed are equally probable. Therefore, no movement is possible on average.

Examine, for instance, the mechanical ratchet system of section 1.1.3, working at a single temperature. Due to fluctuation, during some time interval, the ratchet might be moving forward. But, due to detailed balance symmetry, the reversed process is equally likely, and by waiting long enough another fluctuation making the ratchet rotate backward should occur.

It is therefore a symmetry condition, detailed balance, which is behind the absence of (average) motion at thermal equilibrium, not minding the spatial asymmetries present in the system.

## 1.2 Fundamental Models of Ratchet Devices

We have seen so far that asymmetry alone cannot sustain the operation of a Brownian motor. The system must also be taken out of equilibrium. This is done by keeping both metals in the diode of the Brillouin paradox at different temperatures. For the case of Feynman's ratchet, it is the vanes and the wheel that are at different temperatures. Keeping them at different temperatures is easy because these are macroscopic

systems. It however becomes difficult to keep two parts of a microscopic or molecular level system at different temperatures. These systems are the most interesting for the realization of the Brownian ratchet. In fact, in these microscopic systems, thermal fluctuations are generally not negligible at all but crucial.

There are different ways to keep the system away from thermal equilibrium. The fundamental ones are three in numbers, the flashing or pulsating ratchet, the forced or rocking ratchet, and the information or feedback ratchet. The flashing ratchet was initiated by Ajdari and Prost (1992) [7] and has had a large influence in the scientific community, prompting many experimental and theoretical works. It has a time-dependent perturbation in the potential shape. The forced ratchet with an additive and unbiased driving force was realized by Magnasco (1993) [8]. The idea of information ratchet was initiated by Astumian and Derenyi (1998) [9] to explain chemical powered motor like the motor proteins present in all living thing beings. In the information ratchet, the perturbation depends on the previous position of the particle.

These fundamental ratchet systems may have some variations and generalization, e.g. a larger number of spatial dimensions, a non-equilibrium perturbation that is not time-periodic but random, nonlinear friction forces, etc. However, the primary mechanisms are not different from the above-mentioned fundamental models of ratchet systems.

The potential of the cold atom ratchet is a flashing ratchet. We are going to look at the flashing ratchet in a more detailed way. The other two can be found in [10].

### 1.2.1 The Flashing Ratchet

Let us look at a 1-D dynamics of a Brownian particle moving in the x-direction in the presence of a ratchet potential V(x) – spatially asymmetric and spatially periodic $V(x + L) = V(x)$ as seen in the top panel of Fig 1.4. Though the spatial inversion symmetry is broken by the asymmetric potential, it is not enough for us to get on average a directed motion if the system is at thermal equilibrium – this we are

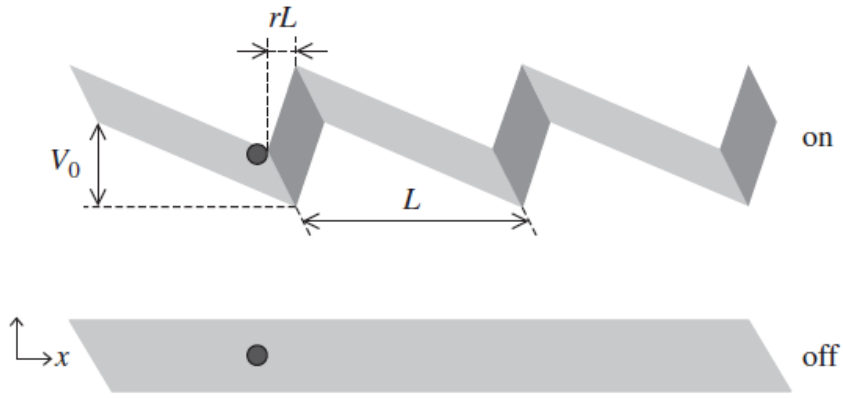


Fig 1.4 Flashing ratchet: the potential experienced by a Brownian particle, switches between an on state, with an asymmetric, ratchet-like shape, and an off state, where the particle diffuses freely. The dimensionless parameter marks the asymmetry of the potential, with r ≠ ½ for an asymmetric potential.

cleared about already. Quantitatively, the statistical average of velocity,

$$\langle v \rangle = \lim_{t\to\infty} \frac{1}{t} \int_0^t dt' \left(\frac{dx(t')}{dt}\right) = \lim_{t\to\infty} \frac{<x(t) - x(0)>}{t} \qquad (1.6)$$

As the particle interacts with the environment, it reaches thermal equilibrium and this is modeled using frictional force with a force constant $\gamma$ and a random force $\xi$(t). We assumed that the stochastic force comes from a Gaussian white process and thus, $\xi$(t) has a zero mean

$$< \xi(t) > = 0 \qquad (1.7)$$

and a second moment of the form

$$< \xi(t)\, \xi(t') > = 2\Gamma\delta(t - t') \qquad (1.8)$$

The stochastic equation of motion of the Brownian particle, of mass m, is

$$m\frac{d^2x}{dt^2} = -\gamma\frac{dx}{dt} - \frac{\partial V(x)}{\partial x} + \xi(t) \qquad (1.9)$$

A common circumstance in many experiments is that m/$\gamma$ is much smaller than any other characteristic time in the system – this is called the overdamped regime, and the equation of motion is given by the Langevin equation

$$\gamma \frac{dx}{dt} = -\frac{\partial V(x)}{\partial x} + \xi(t) \tag{1.10}$$

The damping is so strong in this regime that the Brownian particle quickly gets to the terminal velocity given by equation (1.10) every time. With this assumption of our system at thermal equilibrium, the fluctuation-dissipation theorem $\Gamma = \gamma K_B T$ is valid – the noise strength is directly proportional to the friction coefficient $\gamma$ and the absolute temperature T.

In the limit of deep potential i.e.$K_B T << V_0$, the Brownian particle is mostly trapped at the bottom of one of the potential wells, as shown in the upper panel of Fig 1.4. To have a directed motion, we have to drive the system out of equilibrium, and it is done by using a non-stationary potential. The potential is kept on for a time $\tau_{on}$ and then switched off for a time $\tau_{off}$. To make our analysis simple enough, we will assume $\tau_{on}$ to be long enough so that the Brownian particle will have enough time to settle at the bottom of the well in which it was at the beginning of the phase. During the times $\tau_{off}$, the particle diffuses freely, following

$$\gamma \frac{dx}{dt} = \xi(t) \tag{1.11}$$

After this phase of free diffusion, the potential is switched back on. Thus, the system works in a cycle just like a heat engine. For the interval $\tau_{off}$, the particle covers an average distance given by the normal diffusion equation

$$\langle [x(t) - x_0]^2 \rangle = 2D\tau_{off} \tag{1.12}$$

Where $x_0$ is the initial position – at the bottom of the potential – and the spatial diffusion coefficient D is specified by $D = K_B T/\gamma$ (Einstein relation). A suitable choice of $\tau_{off}$ is gotten by considering the

probability of the particle displacement in the right and left direction. We take $\tau_{off}$ to be large enough to allow the particle sufficient time to travel a distance $rL$, passing the barrier position of the on-state situated at the right of the initial well, but small enough to prevent Brownian particle from traveling a distance $(1-r)L$ and hence cannot pass the position corresponding to the left of the initial well. From equation (1.12), it implies that $\tau_{off}$ should be

$$\frac{(rL)^2}{2D} \cong \tau_{off} \ll \frac{(1-r)^2L^2}{2D} \tag{1.13}$$

a condition that is valid for $r \ll 1$. Then, at the inception of the next on-state interval, the particle will have a higher probability of being within the well at the right of the original one than at its left. Additionally, the Brownian particle will have an insignificant probability of traveling more than one well.

During the on-state, the particle will again be retrapped at the minimum of the well. $\tau_{on}$ can be taken long enough to allow for a complete retrapping of the particle at the minimum of the potential well. Immediately the potential is switched on, the particle will be exerted on by a steady force $V_0/(1-r)L$ pushing it towards the next potential minimum at the right. Thermal fluctuation is negligible since $K_BT \ll V_0$. For a particle starting near the upper point of a potential barrier at the inception of the on-state time interval, from equation (1.10) the average time to get to the minimum is $\gamma(1-r)^2L^2/V_0$. This is exactly the time needed for the particle to be retrapped at the bottom of the well, hence

$$t_{on} \geq \gamma(1-r)^2L^2/V_0 \tag{1.14}$$

can be regarded to optimize the ratchet device.

The normal diffusion and retrapping phases combined brought about motion with a high probability from the original position $x_0$ to the final position $x = x_0 + L$. As this repeats, the system is set to move in the positive direction (this is directed transport).

The above-mentioned logic also directly opens on to an estimate for the average velocity. As the off-state comes to an end the probability density of finding the particle at a distance $x - x_0$ from the potential minimum $x_0$ is

$$p(x, \tau_{off}) = \frac{1}{\sqrt{4\pi D\tau_{off}}} exp\left(-\frac{(x-x_0)^2}{\sqrt{4D\tau_{off}}}\right) \quad (1.15)$$

In the condition defined by equation 8, during the off-state, the particle has a high probability of traveling past the position of the potential barrier on the right of the original site, and a very insignificant probability of passing the position of the first barrier on the left or even the second on the right. Thus, the probability that the particle has diffused to the right well is

$$p_r = \int_{rL}^{\infty} dx\ p(x, \tau_{off}) = \frac{1}{2} erfc\left(\frac{rL}{\sqrt{4D\tau_{off}}}\right) \quad (1.16)$$

For instance, if we choose $\tau_{off} = (rL)^2/2D$, we will get $p_r = erfc(1/\sqrt{2}) = 0.1586\ldots$ Since in each cycle, the particle moves a distance $L$ to the right with probability $p_r$, the mean velocity will be

$$\langle v \rangle = \frac{p_r L}{\tau_{on} + \tau_{off}} \quad (1.17)$$

The flashing ratchet is a unique rectifier of thermal fluctuations from only one temperature source. If there are no fluctuations, i.e. $T = \Gamma = 0$, then we will have zero current $\langle v \rangle = 0$. The asymmetric potential during the on-state $\tau_{on}$ is rectifying the thermal fluctuations connected with the free diffusion in the preceding off state.

It should be noted that this examination of the flashing ratchet was confined to the regime $K_B T \ll V_0$, equation (1.13) and equation (1.14) regime, to get a clear description of its working mechanism, and also to derive a simple expression for the current. Flashing ratchet however generates a current over a much broader range of parameters, and can also work for random on and off times, and also for partial suppression of the ratchet potential.

The directed motion of the flashing ratchet comes from the time-dependent variation in the potential landscape, which requires sustained energy input. Also, the second law is not breached, thermal equilibrium was only avoided. On the other hand, this does not mean the thermal fluctuations are inconsequential in the operating mechanism of this prototypal Brownian motor.

We have so far been discussing single-particle transport in the classical regime because the regime describes dynamics perfectly at the molecular level and when the temperature is moderate (such as room temperature) where Newton's law governs the dynamics of atoms and molecular motion. Although quantum mechanics is needed to explain the interaction potentials between these atoms, the dynamics are strictly classical. Some of the most intriguing ratchet regimes, one of which is the biological molecular motors, is behind the mechanical movement of living things is in this regime.

Besides biological machines which are majorly in the classical regime, Brownian ratchets have also the quantum regime. The scope of this work is in this second regime – quantum ratchets (where genuine quantum effects like tunneling give rise to new transport mechanisms e.g. tunneling-induced current reversal) inspire the artificial design of nano-engines.

### 1.3 General Relevance of the Concept of Ratchets

1. The Realm of the World at the Nanoscale:

   Brownian ratchet has influenced or inspired the field of nanotechnology as the effect of noise and thermal fluctuation is felt on a small scale. At room temperature, atoms are incessantly hitting each other resulting in a Brownian motion. Its motion is governed by classical dynamic with noise.

2. Molecular Motors:

These are microscopic biological machines that determine the motion in a cell. They move in one direction just as in the ratchet device. The motor protein is a group of molecular motors that are behind

the transport of substances within the cell, the mechanism of the body muscles, movement of cells, and other activities during cell division.

The non-equilibrium concentration of Adenosine triphosphate, ATP is a way to bring motor protein out of equilibrium to satisfy the second law of thermodynamics. When ATP reacts with water (ATP hydrolysis), it decomposes into Adenosine diphosphate, ADP, and a hydrated phosphate $P_i$, and liberating energy of approximately $14K_BT$.

The mitochondria which are the "power plants" of the cell are steadily recycling the used ADP and $P_i$, changing them into fresh ATP, and thus, increasing the concentration of ATP to a value much higher than its thermal equilibrium value. Another way ATP is produced is through a molecular motor known as ATP synthase which uses energy gotten from food to recompose ATP.

Note that the energy gotten from hydrolyzing ATP is not directly utilized to drive the motor in its directional motion. It only gives a requisite step to complete the cycle, the same function served by the non-equilibrium, time-dependent changes of the potential terrain in the flashing ratchet earlier discussed. Though they may not be biasing the directed motion, they are indispensable both to take the system out of equilibrium and to supply the needed input energy.

Amidst the motor proteins, we have three large families of linear motors that move along a filament. The first families are the myosins. They move along actin filaments, and they are responsible for muscle contraction. The second and the third families are the kinesins and the dynesins respectively. They walk on microtubules inside the cell conveying cargo or aiding cell division.

### 1.4 Cold Atoms Ratchets

Cold atoms in optical lattices are a perfect testbed to walk around ratchet physics. This is mainly due to the great tunability of optical lattice systems, which permits one to precisely control the shape of the potential and of whichever applied force, as well as to change at will the intensity of dissipation. Since the

very original demonstration of directed motion in a cold atom system by Mennerat-Robilliard et al. (1999), several experimental investigations with cold atoms in optical lattices have explored diverse features of the physics of ratchets. Here, the focus is on the full quantum Hamiltonian regime.

Optical lattices are periodic potentials for atoms made by the interference of two or more laser fields. The detuning between the laser fields and the nearest atomic transition will come out as a key parameter to explain the light–atom interaction. It is thus necessary to differentiate two very dissimilar situations: the case of far-detuned laser fields, and the case of near-resonant laser fields. For far-detuned laser fields, an entirely conservative potential is produced. Far-detuned optical lattices are perfect to model Hamiltonian systems. In the case of near-resonant laser fields, the interaction between the laser and the atoms may lead, under proper settings, to dissipative dynamics. That is, for a properly arranged set of near-resonant optical lattices, a *dissipative* optical lattice, is created, where the set of laser fields create at once the periodic potential acting on the atoms and the cooling process, which reduces their kinetic energy and result in the trapping of the atoms at the base of potential wells.

### 1.5 Goals of this Work

We have seen how the flashing on and off of our asymmetric ratchet potential can lead to directed transport. I mean how this out-of-equilibrium mechanism leads to an average motion in just one direction. But the question is how can we increase the current rate? What are the ways we could enhance this unidirectional transport? Noise can be disadvantageous in a system as well as advantageous. In trying to answer these questions, we want to see if we can avail of our system's current rate with amplitude noise. We want to see the effect of implementing amplitude noise into our system on our current rate and energy. We try to increase the noise level for different values of kick strength and watch how it promotes our current rate. Lastly, we will look at the momentum distribution curve and see if it also supports enhanced transport.

## CHAPTER TWO

## THEORETICAL BACKGROUND

Quantum ratchets show properties that are qualitatively different from their classical counterparts. For instance, quantum tunneling may cause an unexpected current reversal.

We have two classes of quantum ratchets: the dissipative quantum ratchet and the Hamiltonian quantum ratchet. The dissipative quantum ratchets are a quantum form of stochastic ratchet where fluctuations and dissipation are present. The dynamics of the dissipative quantum ratchet are governed by the quantum Langevin equation [10].

$$m\ddot{\hat{x}}(t) = -\gamma\,\dot{\hat{x}}(t) - V'\big(\hat{x}(t)\big) + F(t) + \hat{\xi}(t) \tag{2.1}$$

where the prime and the dot denote space and time derivatives respectively. Equation (2.1) looks very identical to the classical Langevin equation except that $\hat{x}(t)$ is the coordinate operator and $\hat{\xi}(t)$, the quantum noise operator, both in the Heisenberg picture.

Our focus is on the second class of quantum ratchet, the quantum Hamiltonian ratchet where fluctuations and dissipation are absent. This research is very much related to the study of the quantum kicked rotor which can be experimentally achieved in a symmetric optical-lattice potential that is flashed on and off periodically in time. A quantum flashing ratchet, which we examine here is a generalization of the kicked rotor to an asymmetric potential.

For a nonlinear quantum pump acting on a particle in an optical lattice driven by a flashing mechanism, we are going to show the derivation of its dimensionless time-dependent Schrodinger equation from the dimensional form.

The time-dependent Schrodinger equation is

$$i\hbar\frac{\partial\psi}{\partial t} = H\psi \tag{2.2}$$

where the Hamiltonian H is given as

$$H = \frac{p^2}{2m} + V_0[\sin(2k_L x) + \alpha \sin(4k_L x)] \sum_{n=0}^{\infty} \delta(t - nT) \quad (2.3)$$

where T is the flashing period. That means the light is being switched on and off periodically. $\omega = \frac{1}{T}$. Also, $V_0$ is the amplitude of the periodic potential.

Let

$$x' = 2k_L x; \qquad p' = \frac{2k_L}{m\omega} p; \qquad t' = \omega t = \frac{t}{T} \quad (2.4)$$

Substituting (2.4) into the Hamiltonian (2.3), we have

$$H = \frac{m\omega^2 p'^2}{4k_L^2} \frac{1}{2} + V_0[\sin(x') + \alpha \sin(2x')] \sum_{n=0}^{\infty} \delta(T(t' - n)) \quad (2.5)$$

Multip;ying through by $\frac{4k_L^2}{m\omega^2}$ we get the rescaled Hamiltonian H':

$$\frac{4k_L^2}{m\omega^2} H = \frac{p'^2}{2} + \frac{4k_L^2}{m\omega^2} V_0[\sin(x') + \alpha \sin(2x')] \sum_{n=0}^{\infty} \delta(T(t' - n)) = H' \quad (2.6)$$

The rescaled Hamiltonian is now $H' = \frac{4k_L^2}{m\omega^2} H$

$$H' = \frac{p'^2}{2} + K[\sin(x') + \alpha \sin(2x')] \sum_{n=0}^{\infty} \delta((t' - n)T) \quad (2.7)$$

where $K = \frac{4k_L^2}{m\omega^2} V_0$ (2.8)

Recall that from quantum mechanics the commutator $[x, p] = i\hbar$.

Also, $[x', p'] = \left[2k_L x, \frac{2k_L^2}{m\omega} p\right] = 2k_L . \frac{2k_L^2}{m\omega} [x, p] = \frac{4k_L^2}{m\omega} i\hbar = i\widetilde{\hbar}$ (2.9)

where $\widetilde{\hbar} = \frac{4\hbar k_L^2}{m\omega}$ (2.10)

and $\omega_R = \frac{\hbar k_L^2}{2m}$ is the recoil frequency. It implies that $2\omega_R = \frac{\hbar k_L^2}{m}$. And one finally gets

$$\widetilde{\hbar} = \frac{8\omega_R}{\omega} \tag{2.11}$$

The effective potential strength, $K$ equation (2.8) can be rewritten as

$$K = \frac{4k_L^2}{m\omega}\frac{V_0}{\omega} = \frac{\widetilde{\hbar}}{\hbar}\frac{V_0}{\omega} = \widetilde{\hbar}\frac{V_0 T}{\hbar} \tag{2.12}$$

$$K = \widetilde{\hbar}P \tag{2.13}$$

The corresponding Schrodinger equation can now be written as

$$i\widetilde{\hbar}\frac{\partial\psi}{\partial t} = -\frac{\widetilde{\hbar}^2}{2}\frac{\partial^2\psi}{\partial x^2} + Kv(x)\sum_{n=0}^{\infty}\delta(t-n)\psi \tag{2.14}$$

where $\psi$ is our initial wave function; n is the number of kicks; $v(x)$ is a sawtooth-shaped ratchet potential,

$$v(x) = \sin x + \alpha \sin 2x, \tag{2.15}$$

where $\alpha$ controls the skewness of the periodic potential $\alpha \epsilon$ [0, 0.5] gives a case where the sawteeth lean to the left, leading to a positive current in the usual case of classical diffusive motion. The potential is flashed on and off at periodic intervals. We have taken the pulse to be delta function in time to ease our calculations. For $\alpha$ = 0, we have a kicked rotor. The second sine wave opens up the possibility of a ratchet effect as it adds complexity to the kicked rotor [11].

We have chosen our units in (2.14) so that the spatial period of the lattice and the temporal period of the flashing is unity. Relating the physical quantities, from (2.11), we have the effective Planck constant as

$$\widetilde{\hbar} = 8\omega_R T \tag{2.4}$$

where T is the period of the flashing. The quantum nature of our system is reflected by the effective Planck constant which changes as we change the pulsating period T. Also, $\omega_R = \hbar k_L^2/2m$ is the recoil frequency of the laser field and $k_L$ is the photon wave number and lattice period $(2k_L)^{-1}$ for the optical potential experienced by the atoms. The effective potential strength is given by (2.13). Then, $P = K/\tilde{\hbar}$

A quantum resonance occurs when the period of the flashing is equal to recoil frequency and is related to the arithmetic nature of the effective Planck constant $\tilde{\hbar}$ of the kicked system [12], occurring pointedly if

$$\tilde{\hbar} = \frac{4\pi r}{s} \tag{2.6}$$

with r and s being mutually prime integers. If s is small, it is called low-order quantum resonance (LOQR), and if s is large, it is called high-order quantum resonance (HOQR).

A long coherence width is needed for us to directly observe quantum resonance. The matter is heightened for HOQRs. Not long ago, noncondensed atoms have been indirectly used to observe a certain family of HOQR. However, using Bose-Einstein condensates loaded in optical lattice [13, 14] one can now comfortably get initial quantum states whose coherence spreads across many optical lattice sites, leading to the detection of the main quantum resonance [14] and also quantum resonance of comparatively low orders [13].

The method employed in solving (2.14) will be discussed in chapter 3. It is called the split-operator fast Fourier transform method. In most of the cases, we have assumed an initially homogeneous wave function with zero momentum state: this is a nice approximation for a wave packet that extends over many lattice sites. Another case is when the initial state is an eigenstate of the static potential.

# CHAPTER THREE

# METHODOLOGY

## 3.1 The Split-Operator FFT Method

Though there are different methods to solve our time-dependent Schrodinger equation. The approach used in this work is the split-operator FFT method and was developed by Feit and Fleck in the 1980sl We begin this approach by representing the time-evolution propagator over the time interval [0, t] as a product of propagator over short but finite time steps $\Delta t$, where N $\Delta t$ = t [22]. Therefore,

$$U(t,0) = e^{-\frac{iHt}{\hbar}} = \underbrace{e^{-\frac{iHt}{\hbar}} e^{-\frac{iHt}{\hbar}} \dots e^{-\frac{iHt}{\hbar}}}_{N\ times} \tag{3.1}$$

The split-operator method is based on which approximate way is the time-evolution performed by using the Zassenhaus formula

$$e^{\hat{x}+\hat{y}} = e^{\hat{x}} e^{\hat{y}} e^{-\frac{1}{2}[\hat{x},\ \hat{y}]} e^{-\frac{1}{3}[\hat{y},\ [\hat{x},\ \hat{y}]]} e^{-\frac{1}{6}[\hat{x},\ [\hat{x},\ \hat{y}]]} \dots \tag{3.2}$$

A dual relation is the Baker-Campbell-Haussdorff (BCH) formula and it reads

$$\exp[\hat{x}]exp[\hat{y}] = \exp\{\hat{x} + \hat{y} + \frac{1}{2}[\hat{x},\ \hat{y}] + \frac{1}{12}([\hat{x},\ [\hat{x},\ \hat{y}]] + [\hat{y},\ [\hat{x},\ \hat{y}]]) + \dots\} \tag{3.3}$$

We limit the system to a particle moving in 1-D under a Hamiltonian of the typical form H = $T_k$(p) + V(x). For very short time intervals $\Delta t$, one then obtains from the Zassenhaus formula that

$$e^{-\frac{i\hat{H}\Delta t}{\hbar}} approximately\ e^{-\frac{i\hat{T}_k\Delta t}{\hbar}} e^{-\frac{i\hat{V}\Delta t}{\hbar}} \tag{3.4}$$

is accurate to first order in $\Delta t$, We can prove that a more symmetrical splitting of the Hamiltonian

according to

$$e^{-\frac{i\hat{H}\Delta t}{\hbar}} = e^{-\frac{i\hat{V}\Delta t}{2\hbar}} e^{-\frac{i\hat{T}_k\Delta t}{\hbar}} e^{-\frac{i\hat{V}\Delta t}{2\hbar}} + O(\Delta t^3) \tag{3.5}$$

Leads to an approximation of higher accuracy

The problem of which (finite) basis is used to represent the wave function is solved by representing it at t = 0 on a position space grid $x_n \in [x_{min}, x_{max}]$ n = 1, . . . ,N. The wave function evolved for a time step $\Delta t$ at the grid point $x_n$ is then stated as

$$\psi(x_n, \Delta t) = \left\langle x_n \middle| e^{-\frac{i\hat{H}\Delta t}{\hbar}} \middle| \psi(0) \right\rangle \approx \left\langle x_n \middle| e^{-\frac{i\hat{V}\Delta t}{2\hbar}} e^{-\frac{i\hat{T}_k \Delta t}{\hbar}} e^{-\frac{i\hat{V}\Delta t}{2\hbar}} \middle| \psi(0) \right\rangle \tag{3.6}$$

By inserting unity two times in terms of position state and one time in terms of momentum states, the threefold integral (using numerical method, the integration are in discrete form since our wave function will be on a grid)

$$\psi(x_n, \Delta t) \approx \int dx' \int dp' \int dx'' \left\langle x_n \middle| e^{-\frac{i\hat{V}\Delta t}{2\hbar}} \middle| x'' \right\rangle \left\langle x'' \middle| e^{-\frac{i\hat{T}_k \Delta t}{\hbar}} \middle| p' \right\rangle \left\langle p' \middle| e^{-\frac{i\hat{V}\Delta t}{2\hbar}} \middle| x' \right\rangle \langle x'|\psi(0)\rangle \tag{3.7}$$

comes out. The integral over x'' can be from straight away due to the locality of the potential in position space and the $\delta$ function coming in.

$$\left\langle x_n \middle| e^{-\frac{i\hat{V}\Delta t}{2\hbar}} \middle| x'' \right\rangle = e^{-\frac{i\hat{V}(x')\Delta t}{2\hbar}} \delta(x' - x_n) \tag{3.8}$$

Also the second exponentiated potential term simplifies as a result of locality according to

$$\left\langle p' \middle| e^{-\frac{i\hat{V}\Delta t}{2\hbar}} \middle| x' \right\rangle = \langle p'|x'\rangle e^{-\frac{i\hat{V}(x')\Delta t}{2\hbar}} = \frac{1}{\sqrt{2\pi\hbar}} e^{-\frac{ip'x'}{\hbar}} e^{-\frac{i\hat{V}(x')\Delta t}{2\hbar}} \tag{3.9}$$

The Fourier transformation of the "in-between or intermediary wave function" into momentum space is represented as the x' integration. As a result of this, our exponentiated operator kinetic energy becomes local and can be easily applied through

$$\left\langle x'' \middle| e^{-\frac{i\hat{T}_k \Delta t}{\hbar}} \middle| p' \right\rangle = \langle x''|p'\rangle e^{-\frac{i\hat{T}_k(p')\Delta t}{\hbar}} = \frac{1}{\sqrt{2\pi\hbar}} e^{-\frac{ip'x''}{\hbar}} e^{-\frac{i\hat{T}_k(p')\Delta t}{\hbar}} \tag{3.10}$$

The p' integration changes the wave function but into position space

The main numerical work is the demand to do two Fourier transforms of the wave function during the evolution over one time step. This can be done by making use of the fast Fourier transformation (FFT) algorithm. We can thus summarize the implementation of the split-operator based FFT method as follows [23]:

1. Discretize the initial wave function by representing it on a position space grid.
2. Apply the local operator $e^{-\frac{i\widehat{V}\Delta t}{2\hbar}}$
3. Perform an inverse FFT into momentum space
4. Apply the local operator $e^{-\frac{i\widehat{T}_k\Delta t}{\hbar}}$
5. Perform an FFT back into position space
6. Apply the local operator $e^{-\frac{i\widehat{V}\Delta t}{2\hbar}}$

This course of action is applied for the propagation of small $\Delta t$. For the case where the propagation is over long times it will be recurringly repeated and if the intermediary values of the wave function are not required, the two half-time with propagation under V coalesce (except the first and last one).

Also, we emphasize that to propagate the wave function over the next $\Delta t$, we will require its value not only at some $x_n$ but at all values of x. This tells us about the *nonlocal* nature of quantum theory which is a distinction between quantum theory and classical mechanics. The latter is a local theory since a trajectory depends on its initial conditions.

Some details of the FFT is given as follows. A function $\phi(x_n)$ can be written as a discrete Fourier transform according to

$$\Phi(x_n) = \frac{1}{N}\sum_{k=-\frac{N}{2}+1}^{N/2} a_k e^{2\pi i k x_n/L} \tag{3.11}$$

with the discrete inverse transform

$$a_k = \frac{1}{N}\sum_{n=1}^{N} \Phi(x_n)\, e^{2\pi i k x_n/L} \tag{3.12}$$

To execute this, it is necessary to note this

- N has to be a power of 2, i.e., $N = 2^j$
- The grid length is $L = x_{max} - x_{min}$ and $x_n$ are equidistant with $\Delta x = LN$
- The numerical effort scales with NlnN
- The maximal momentum is $p_{max} = h/2\ \Delta x = Nh/2L$ and $p_{min}$ and $-p_{max}$
- The covered plane space volume is $V_p = 2Lp_{max} = Nh$
- The time step should $\Delta t < \hbar\pi/3V_{max}$ with $V_{max}$ the maximum excursion of the potential.
- The energy resolution is given by $\Delta E_{max} = h\pi/T_t$ where $T_t$ is the total propagation time.

There are further contemporary implementations of FFT which do not require that N to be an integer power of 2, and through some adaption makes the process faster (FFTW: fastest Fourier transformation in the West).

One drawback of the split-operator method is that the method only triumphs in constructing local operators if there are no products of momenta and coordinates operator in the Hamiltonian, such as an operator of the form $e^{i\hat{p}\hat{x}}$.

### 3.1.1 Negative Imaginary Absorbing Potential

Another likely disadvantage of a grid-based approach like the split-operator FFT method shall be discussed in a bit more detail. What happens to a wave packet, when it strikes the grid boundaries? It would reappear on the other side of the grid resulting to nonphysical results! This can be prevented by adding a negative imaginary absorbing potential of the form

$$V(x) = -if(x)\Theta(x - x_n) \tag{3.13}$$

which is now equal to zero for values of $x > x_n$, close to the right grid boundary $x_{max}$. This is also similar to the left side of the grid. There is a loss of norm because our total potential is now complex. However, this problem is not as challenging as the reentrance occurrence, particularly in circumstances of "free space" like in a scattering setting after the scattering incident is over.

Choosing the functional form of $f(x)$ in equation (3.13) is critical. The potential had to rise smoothly and quite slowly to avoid unphysical reflection of the wave function induced by the absorbing potential. [24] has a detailed review of some functional form of the imaginary potential.

Using this split-operator FFT method, I was able to reproduce results found in the literature. These previous results will be discussed in the next section.

### 3.2 Time Evolution

Momentum or current: This is computed in the usual way as the expectation value of the wavenumber or the momentum. Thus, the momentum, also called current is written as $\langle k \rangle = \langle \psi(t)|k|\psi(t) \rangle$

Also, the energy of the system is computed as the current, the expectation value of the square of the wave number which is proportional to the energy of our particle. The time evolution is given by $\langle k \rangle = \langle \psi(t)|k^2|\psi(t) \rangle$

We have taken $\alpha$, the potential asymmetry to be 0.3 all through. Also, we assume our initial wave function to be the uniform zero-momentum state. The topmost panel of Fig 3.1 show a generic non-transporting case $\tilde{\hbar} = 0.711\pi$ and $\tilde{\hbar} = 0.232\pi$ since the momentum averages out to zero at long times. It is in agreement with the finding of [11] which has that for a generic choice of parameter $\tilde{\hbar}$ and P, there is no long-time directed transport when noise is absent. We note that we assumed a rather weak potential strength P = 0.5 in this case.

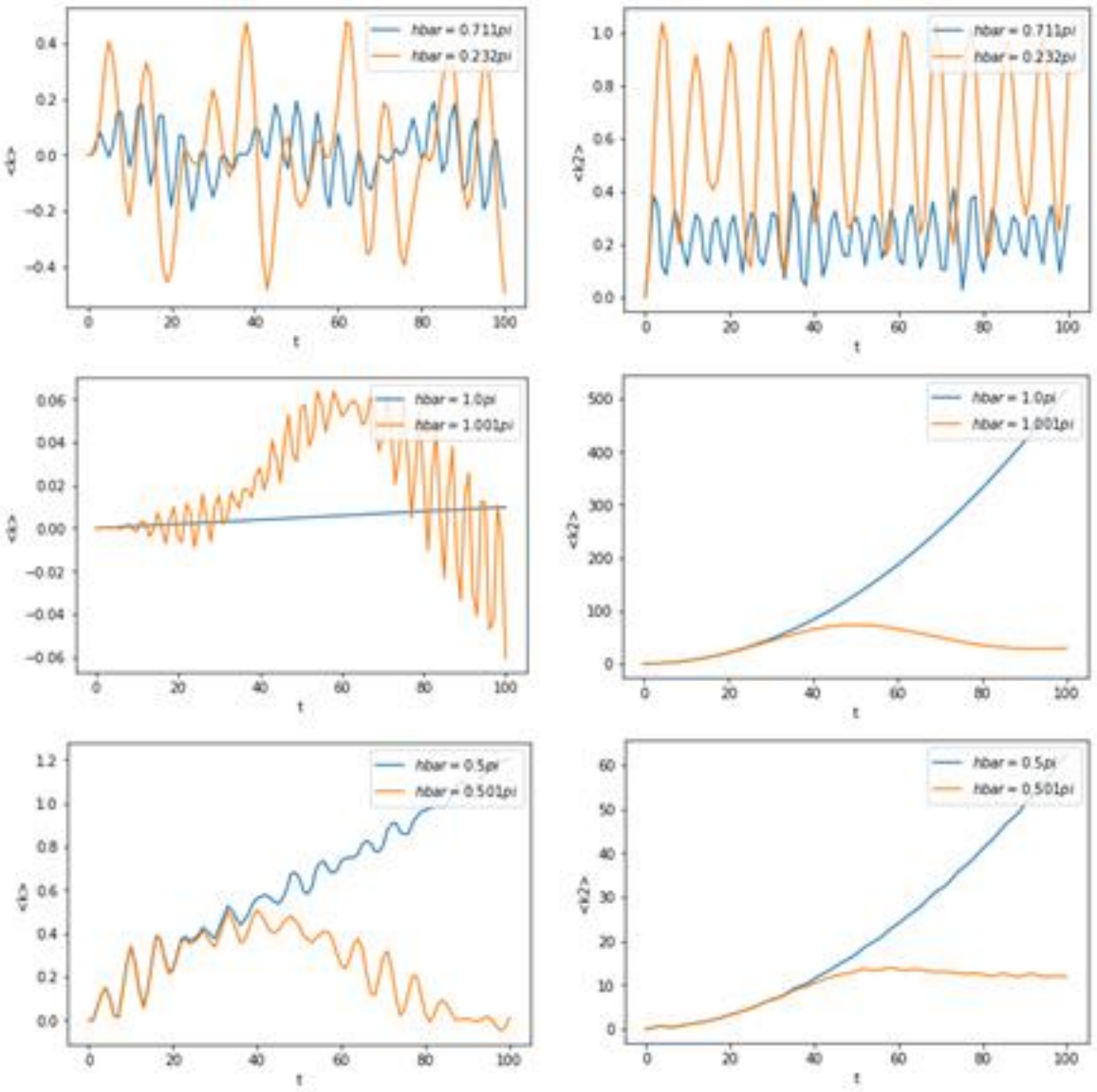


Fig 3.1 Time development of the wavenumber <k> and the square wave number for several parameter choices. In all cases the potential strength P = 0.5 and the asymmetry $\alpha$ = 0.3. In the topmost two panels, the blue line represents the choice with $\tilde{\hbar}$ = 0.711$\pi$ and the red line is $\tilde{\hbar}$ = 0.232$\pi$. In the middle panels, the blue line represents $\tilde{\hbar}$ = 1.0$\pi$ and the red line $\tilde{\hbar}$ = 1.001$\pi$. In the bottom panels, the blue line represents the choice with $\tilde{\hbar}$ = 0.5$\pi$ and the red line $\tilde{\hbar}$ = 0.501$\pi$.

### 3.3 Resonances

The story is different when $\tilde{\hbar}$ is a rational multiple of $\pi$. This is a long-studied subject in the case of the quantum kicked rotor [15 - 18], where quantum resonances are seen to lead to a quadratic increase of the

kinetic energy with time. In the case of a ratchet potential, these ratchets open up for the possibility of directed transport. In a case of weak potential, there is a genuine ratchet effect when $\tilde{\hbar}$ is a half-integer multiple of $\pi$ [19] as can be seen in the lowest panels, $\tilde{\hbar} = \pi/2$. This momentum increases linearly with time. This is so because our choice of the initial wave function is a zero-momentum state. For the case of slightly off-resonance, $\tilde{\hbar} = 0.501\pi$, the ratchet effect disappears. The ratchet effect for the case of $\tilde{\hbar} = 0.5\pi$ is driven by quantum resonance and not by noise. In the middle panels, $\tilde{\hbar} = 1.0\pi$, we do not also have a true ratchet effect. As said earlier, one of the features of quantum resonance is the quadratic increase of the kinetic energy with time. This can be seen in the middle right panel for $\tilde{\hbar} = 1.0\pi$ and the lowest right panel for $\tilde{\hbar} = 0.5\pi$. However, there is no transport for the case of $\tilde{\hbar} = 1.0\pi$ as can be seen in the middle left panel (where the mean momentum of the wave packet is zero at all times). Also, for cases of slightly off-resonance, $\tilde{\hbar} = 1.001\pi$ and $0.501\pi$ the momentum averages out to zero (or fluctuates about zero).

In Fig 3.2 (a), $\tilde{\hbar} = 1.001\pi$ we can see that there is no transport even for any value of potential strength. Fig 3.2 (b) – (d) where $\tilde{\hbar} = 0.7\pi$ for (r, s) = (7, 40), $\tilde{\hbar} = 2.625\pi$ for (r, s) = (21, 32) and $\tilde{\hbar} = 1.5\pi$ for (r, s) = (3, 8) respectively, on the other hand exhibit directed transport. Fig 3.2 (b) and 3.2 (c) are HOQRs. Unlike LOQR, there is yet to be a simple explanation of how current depends on $P$ for HOQR. The analytical treatments of HOQR are not simple to deal with, even with perturbation theory using a very small value of $\alpha$ [20].

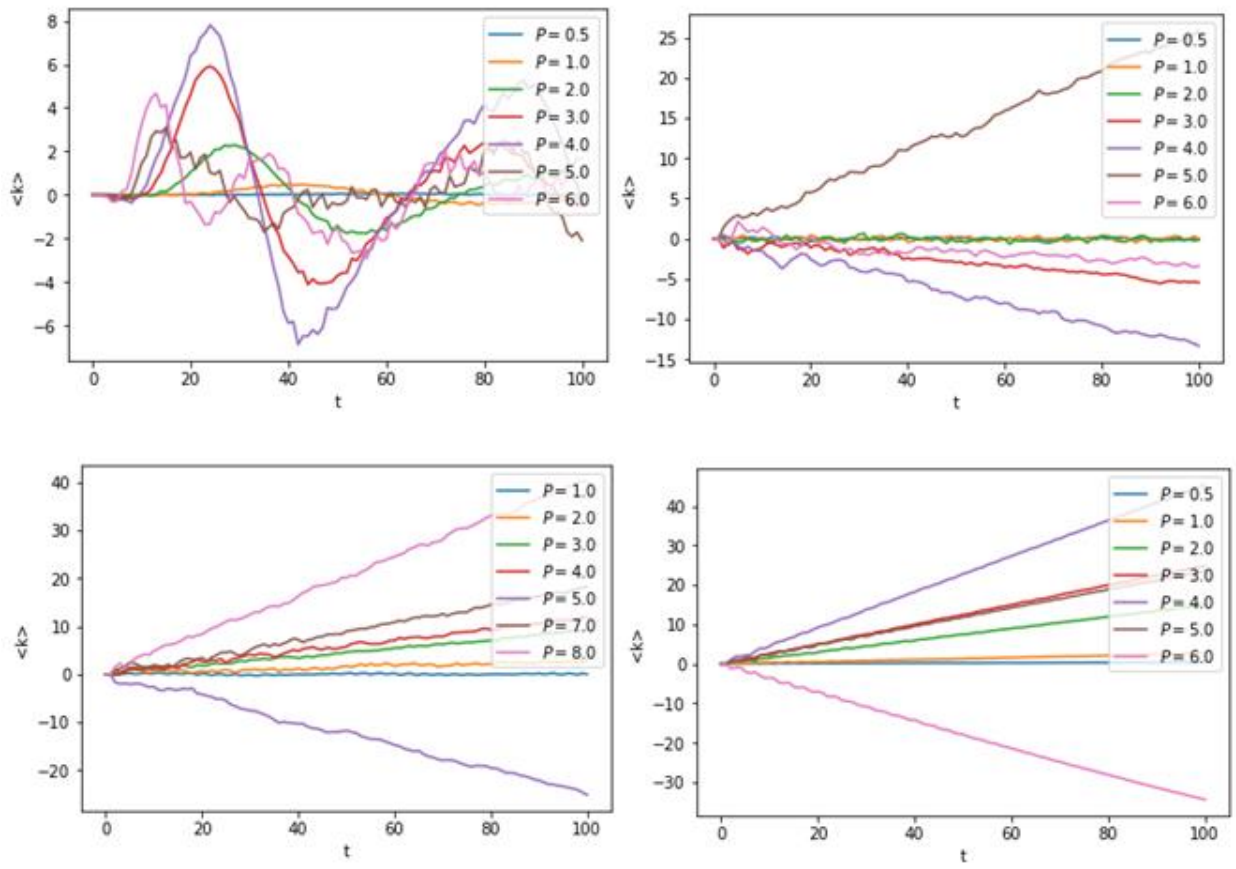


Fig 3.2 Time dependence of the ratchet current for P, $\tilde{\hbar}$. In (a) $\tilde{\hbar}$ =1.001$\pi$ with no directed transport. In (b) $\tilde{\hbar}$ = 0.7$\pi$ (r/s = 7/40), (c) $\tilde{\hbar}$ = 2.625$\pi$ (r/s = 21/32) and (d) $\tilde{\hbar}$ = 1.5$\pi$ (r/s = 3/8) and transport occurs with P-dependent rates and direction.

### 3.4 Initial Conditions

Fig 3.3 shows the time-averaged wavenumber <k>, of the wave packet over time as a function of the effective Planck constant $\tilde{\hbar}$. Again $\alpha$ = 0.3, $P$ = 0.5. The top panel is symmetrized about $\tilde{\hbar}$ = 2$\pi$. This is the homogeneous initial state. The dashed line is a case where the average is taken over the first 20 temporal periods and is not a true ratchet effect but as a consequence of the choice of our initial state. As

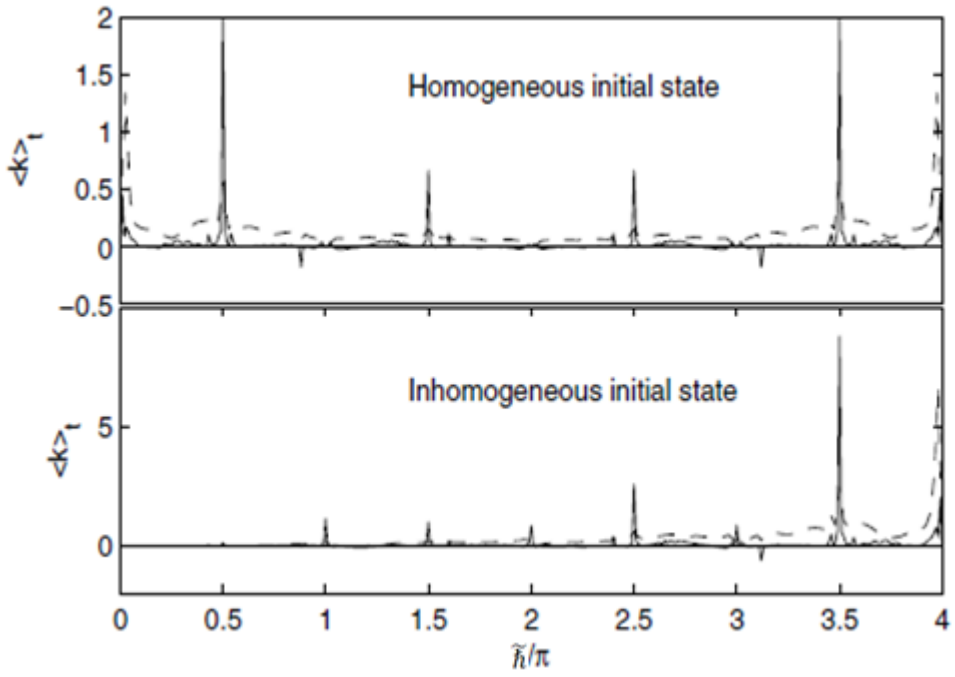


Fig 3.3 Mean wave number of the wave packet over time, as a function of the effective Planck constant $\tilde{\hbar}$. The asymmetry of the potential has been chosen to $\alpha$ = 0.3, and the potential strength $P$ = 0.5. In the topmost panel, the initial state is a homogeneous zero-momentum state and the averaging is done over 20 temporal periods for the dashed line and 100 periods for the solid line. In the lower panel, the initial state was chosen to be the ground state of the potential

the average is taken over 100 temporal periods, a true ratchet effect is visible at half-integer multiples of $\pi$ (i.e., 0.5$\pi$, 1.5$\pi$, 2.5$\pi$, 3.5$\pi$). On the lower panel, we have the case of the inhomogeneous initial state, the ground state of an asymmetric well. Firstly, the figure is not symmetrical like the upper panel. Next, the ratchet effect can be seen at all integers and half-integer multiples of $\pi$, and almost zero current in every other place. The current is positive: this is the anticipated direction for a classical diffusive ratchet in a sawtooth-shaped potential where the teeth tilt to the left.

Ref. [12] reported that for a larger value of $P$, we get the proliferation of peaks. Not only that, but we also get current reversal as can be seen in Fig 3.4 below. Many of these peaks are a result of higher-order quantum resonances covering a wide range of (r, s). As a remark, these high-order resonances may produce larger ratchet current acceleration than the main resonances, and in any of the two cases, the

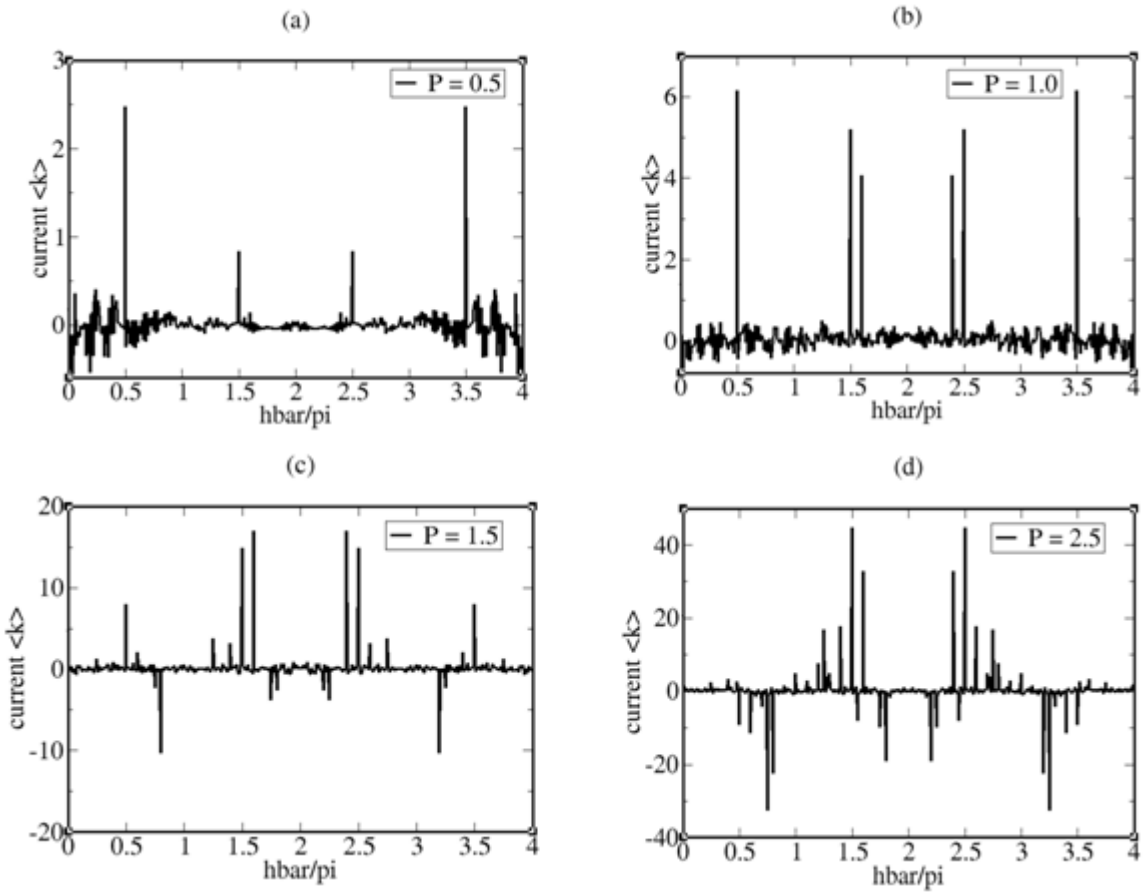


Fig 3.4 Ratchet current <k> as a function of $\tilde{\hbar}/\pi$ after 200 kicks, with the potential parameter $\alpha$ = 0.3, and the potential strength $P$ indicated in each panel. Main resonance appears in (a) with low $P$. As $P$ increases in (b), (c), and (d), full chaos is being developed (see Fig 3.5) and significant ratchet currents due to higher-order quantum resonances emerge.

the current direction depends on P. Note, however that high-order resonances do not always transport better than their low-order counterpart (for instance, from Fig 3.4, compare the HOQR at $\tilde{\hbar}/\pi$ = 0.6 to the LOQR at $\tilde{\hbar}/\pi$ = 0.5, 1.5, 3.5). From Fig 3.4, we can see that by changing $\tilde{\hbar}$ relatively small, we can change the current radically, hence offering a way of separating different HOQRs. This also proposes that particles with slightly dissimilar masses, thus slightly dissimilar $\tilde{\hbar}$ and different $P$ due to an isotope effect, may show qualitatively different types of transport. The resonance peaks of Fig 3.4 are better resolved as we average over more numbers of temporal periods.

Let us look at the corresponding classical dynamics of our system. With the kick strength or classical stochasticity, $K = \widetilde{\hbar}P$, the associated classical map is specified by $p_{l+1} = p_l - K[\cos(x_l) + 2\alpha\cos(2x_l)]$; $x_{l+1} = x_l + p_{l+1}$, where $p_l$ is the momentum conjugate of the coordinate $x_l$. In Fig 3.5, we have the classical phase space for $\alpha$ = 0.3 and for different $K$. As $K$ increases, the islands that are originally dominating the phase space shrink and reduce in number [see Fig 3.5 (a) – 3.5 (c)] until a threshold value $K_{thr}$ when we have full chaos. In Fig 3.5 (d), $K = 0.8\pi > K_{thr}$ approximately $0.75\pi$, the whole phase space is seen to be chaotic.

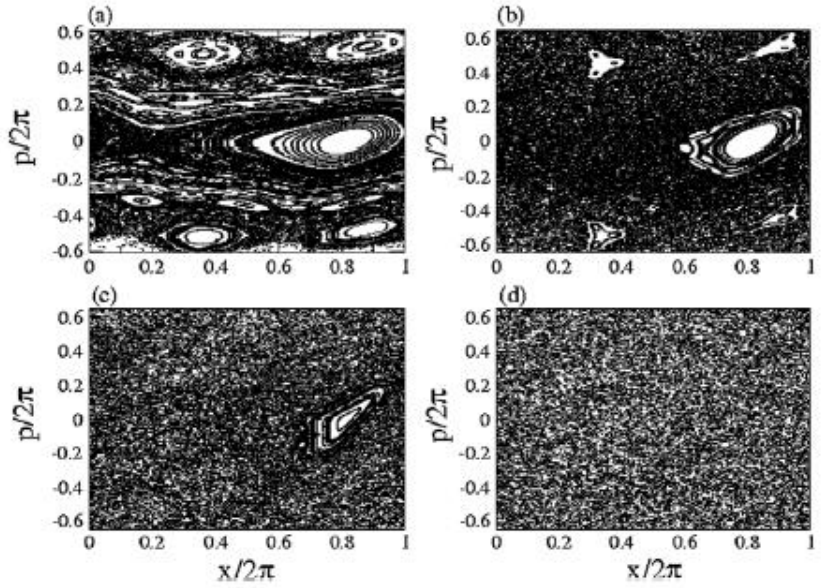


Fig 3.5 Classical phase space structures for the kicked ratchet map for $\alpha$ = 0.3 showing regular islands embedded in the chaotic sea for (a) $K$ = 0.25$\pi$, (b) $K$ = 0.55$\pi$, and (c) $K$ = 0.70$\pi$. In panel (d) $K$ = 0.8$\pi$ and full chaos is reached.

Interestingly, we notice that clear HOQR peaks of the ratchet current appear only when the classical counterpart is entirely chaotic. Such a relationship between purely quantum phenomena and purely classical phenomena is worthy of some comments, however, a deep explanation may not be available. First, quantum resonances result in continuous energy bands. A potential of height $P = K/\widetilde{\hbar}$ supports only a particular number of energy bands (say n) that are below the potential barrier. n $\alpha \sqrt{K}$. For higher

P (i.e., as the well deepens) $K$ becomes higher and consequently increases n. For a fixed $\tilde{\hbar} = K/P$. Larger values of $K$ give rise to more classical chaos and more bands that can bring about transport, hence a higher probability of detecting a HOQR. The outcome of this is more peaks in the plot of the <k> vs $\tilde{\hbar}$. Like this, chaos and HOQRs (both needing significantly large $K$) go hand-in-hand, an interesting result also observed [21] using other signatures.

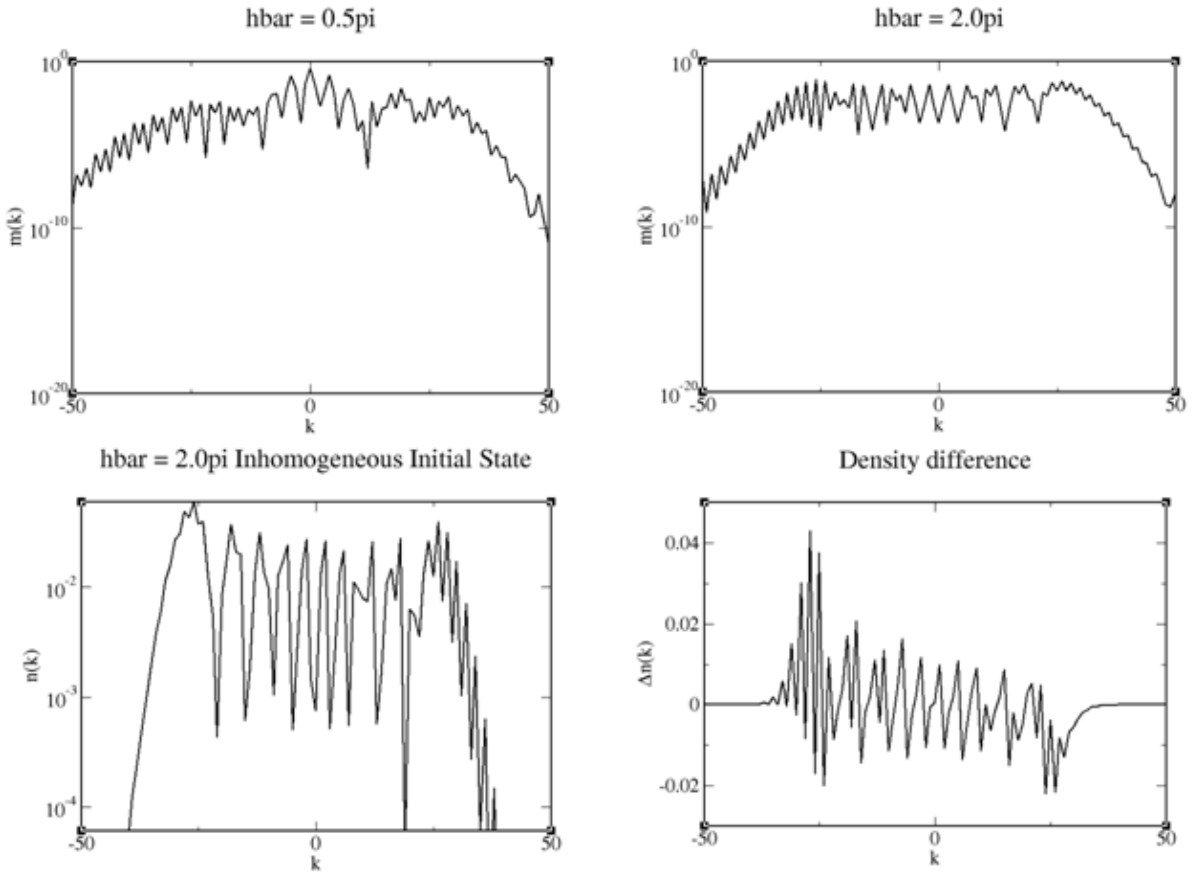


Fig 3.6 Momentum distribution of the wave function. The top left panel displays the momentum distribution for the resonant case $\tilde{\hbar}$ = 0.5$\pi$ after one (dotted line) and 100 kicks (solid line). The initial state was a homogeneous zero-momentum state. The top right panel shows the corresponding result for the case $\tilde{\hbar}$ = 2$\pi$. .The bottom left panel shows the corresponding result for $\tilde{\hbar}$ = 2$\pi$ for inhomogeneous initial conditions, i.e. when the initial state is taken to be the ground state of the potential. The bottom right panel shows the difference between the momentum distribution for $\tilde{\hbar}$ = 2$\pi$ with an inhomogeneous and homogeneous initial condition, $\Delta n = n_{inhom} - n_{hom}$.

On Fig 3.6 are the momentum distributions for the cases of LOQR ($P$ = 0.5). The resonance at $\tilde{\hbar}$ = 0.5$\pi$ shows an asymmetric distribution after 100 kicks. The momentum distribution has a width of the order $10\hbar k_L$, which for the parameter for Ref. [18] amounts to a velocity spread of 10 mm/s. The top-right panel is a homogeneous initial state. We do not have transport at the integer of $\pi$ (in this case $2\pi$). This is why our momentum distribution is symmetric. On the other hand, for the inhomogeneous case, we expect to have current. That is why the momentum distribution in the bottom-left panel is asymmetric. This may not be visible. To make this very noticeable, one must subtract the corresponding momentum distribution for a homogeneous initial condition.

This project is similar to the one we described above. The only difference is that we have introduced amplitude noise into the system since in reality, we cannot avoid this type of noise. Even if it is avoidable, we may introduce them artificially to see if it could enhance our transport. In the next chapter, we will see how we implemented this type of noise into our system.

# CHAPTER FOUR

# AMPLITUDE NOISE

In this chapter, we will see the effect of noise level on the current rate after 100 temporal periods, i.e., we will look at the plots of the current rate against noise level. In the first section, we will briefly discuss the implementation of the amplitude noise into our no-noise system (which has been confirmed to match results in existing literature). In the second section, we have plotted the current rate as a function of noise level for given P and various resonances $\tilde{\hbar}$. And lastly, we will look at the plot of momentum distribution wave function for a given $\tilde{\hbar}$ and $P$, at different noise levels.

## 4.1 Implementation of the Amplitude Noise

In this work, we introduced the amplitude noise by replacing the fixed kick amplitude $P$ which is in the potential energy part of our Hamiltonian with a random, step-dependent amplitude ($P + \delta P_n$), where $\delta P_n$ is a random deviation for the nth kick, uniformly distributed between $-\delta P_{p-p}/2$ and $+\delta P_{p-p}/2$. This random deviation for the nth kick is averaged over 100 realizations. The quantity $\delta P_{p-p}/P$, i.e. the ratio of peak-to-peak deviation to the mean kick amplitude is referred to as the amount of amplitude noise, or simply the noise level. This implementation is similar to the one in [25].

## 4.2 Current Rate vs Noise Level for a Given Potential Strength, *P*

### 4.2.1 Weak Potential Strength, *P* = 0.5 for Different Resonance $\tilde{\hbar}$

In this case of weak potential, we can see how the current rate increased almost linearly with noise level after which it got saturated. For example, in the case of $\tilde{\hbar}$= 0.5pi (the black line), the current rate increases as the noise level increases. The current rate has a maximum value at a noise level of around 270%. Similarly, we can see the green line, the case of $\tilde{\hbar}$= 1.5pi, the current rate increases as the noise level goes up and it has a maximum value when the noise level is approximately 160% after which it decreases

gradually and almost remained constant. A similar trend is seen for the case of $\tilde{\hbar}$ = 2.5pi (the magenta line). In the three cases discussed above, noise enhances our transport. On the other hand, in the cases where $\tilde{\hbar}$= 1.0pi, 2.0pi, and 20.0pi, noise does not have any effect on the current rate. The lines remain on the horizontal axis all through. We are not so perturbed by the result of zero current rates at a 0% noise level. This is expected as already shown and discussed in Fig 3.4: that for a rather weak potential and with an initial homogeneous wave function, we do not get a current for integer multiples of pi.

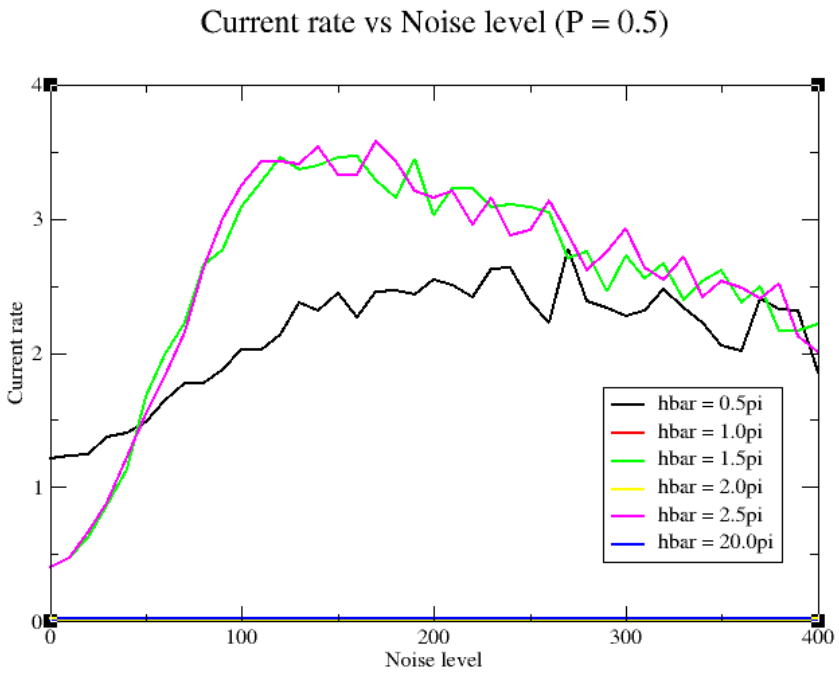


Fig 4.1 The graph of current against noise level for $P$ = 0.5

### 4.2.2 Strong Potential Strength, *P* for Different Resonance $\tilde{\hbar}$

There are some notable features of higher values of potential strength. The first is that noise generally suppresses the current rate to a very low current rate. The second is current reversal. This second attribute is seen for the case where the current direction was originally in the negative current axis, higher values of noise level could help in switching the current to the positive axis so that whether or not the current

started from the positive direction, it will always end in the positive direction as we increase the noise level.

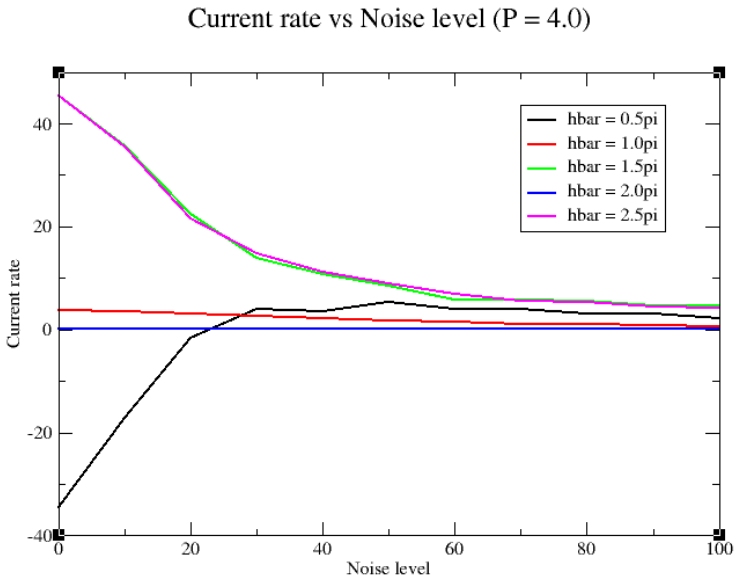


Fig 4.2 The graph of current against noise level for $P$ = 4.0

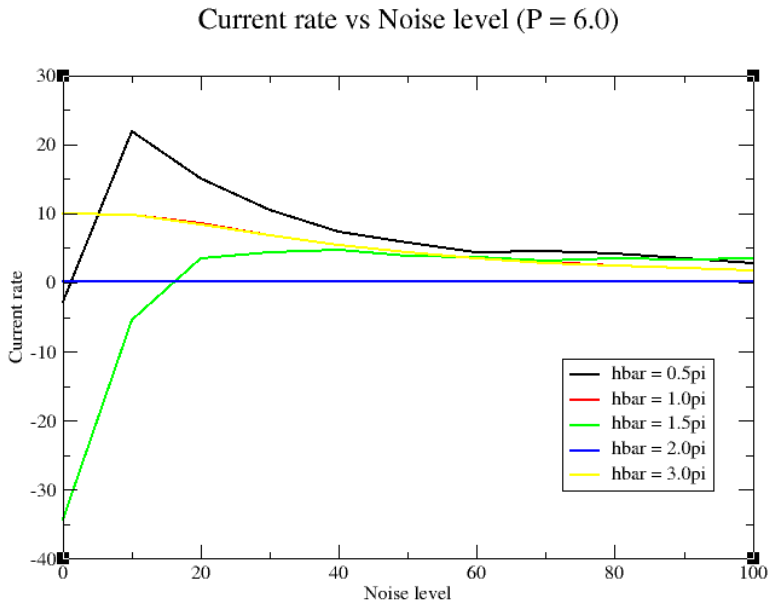


Fig 4.3 The graph of current against noise level for $P$ = 6.0

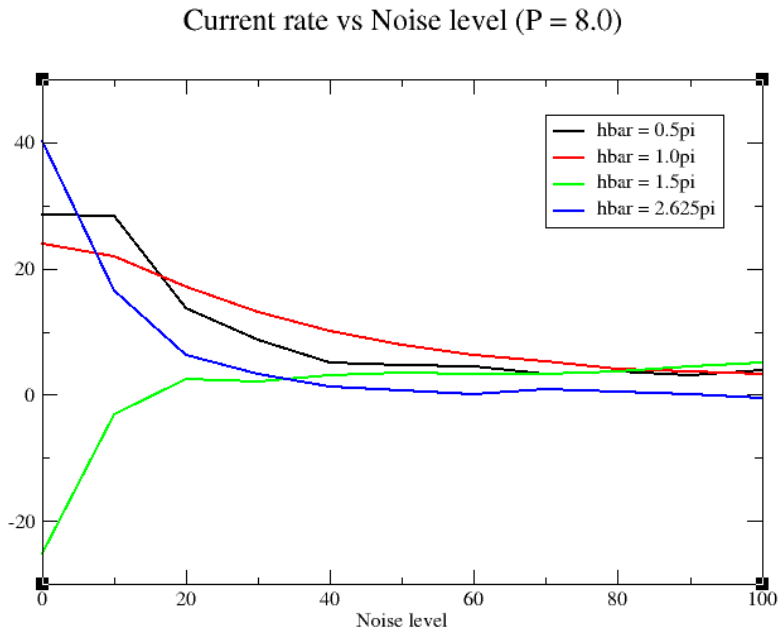


Fig 4.4 The graph of current against noise level for $P$ = 8.0

### 4.3 Momentum Distribution

Just as we discussed earlier for the graph of Fig 4.1: we said that for $\tilde{\hbar}$= 0.5pi, the current rate is minimum for 0% noise level and maximum for a noise level of about 270%. In this section, we look at the momentum distribution curve at these two points. We know that the two curves (black and red) are supposed to be asymmetrical since transport is present in both cases. The asymmetry increases for the case of a noise level of 270%, i.e., the red curve in Fig 4.5. This tells us that the current rate is higher at that noise level. In this same figure, the black curve has a broader momentum distribution when compared with the red curve. This significance is that the case of no noise has a larger window of momenta, that is a larger window of current. In this case, larger currents are allowed within the corresponding window limits. Besides, the black curve has a higher intensity within a momentum range of -10 and +10 units. The physical meaning is that particles within that momentum range are more probable than for the red curve counterpart.

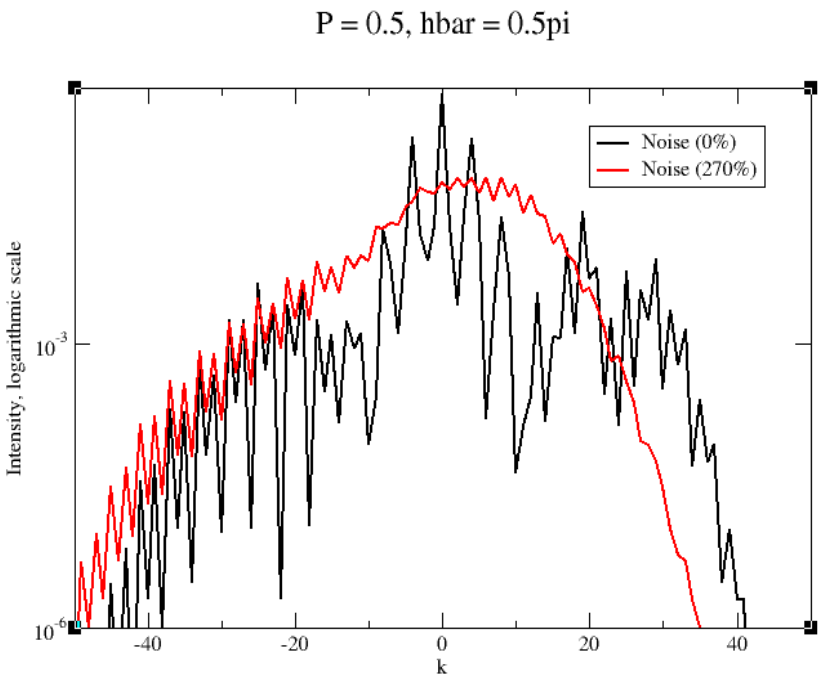


Fig 4.5 Momentum distribution curve for $P$ = 0.5, $\tilde{\hbar}$ = 0.5pi for different noise levels. Black curve is a case of no noise; red curve is a case of 270% noise level.

The same thing can be seen in Fig 4.6, the two curves are asymmetrical as expected, with the case of 160% noise level being more asymmetry indicating a higher current rate. The black curve has a relatively less intensity generally, except for the small momentum range around zero (-5 and +5 unit) where it peaked. It means that the probability of getting the particle with that range of momentum is relatively higher.

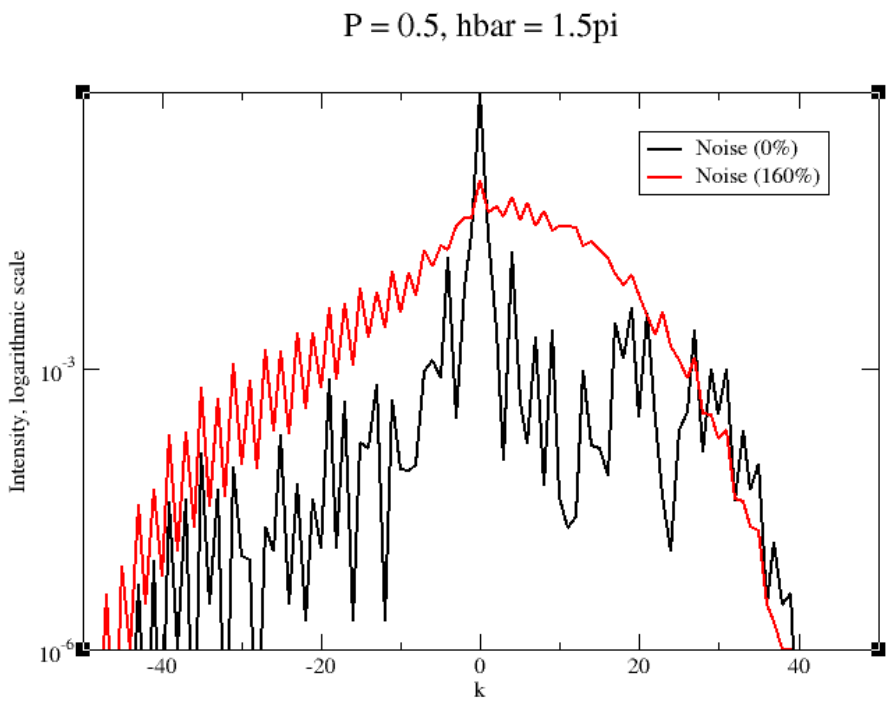


Fig 4.6 momentum distribution curve for $P$ = 0.5, $\tilde{\hbar}$ = 1.5pi for different noise levels. The black curve is a case of no noise; the red curve is a case of 160% noise level.

# CHAPTER FIVE

## SUMMARY AND CONCLUSION

We saw that thermal fluctuation and asymmetry are the two ingredients of a ratchet device. This was clearly stated. Also, moving out of equilibrium is another important condition to get a directed motion. We reviewed a particular fundamental mechanism or operation of ratchet device called the flashing ratchet mechanism. We explained that this mechanism satisfies these three conditions. First, the thermal fluctuations, though the temperature of our Brownian particles is very small compared to the potential depth. The mechanism also satisfies the second condition of asymmetry as the potential landscape leans to one side, maybe to the left. And lastly, the condition of out of equilibrium, where the potential landscape is changing periodically with time. I mean the flashing on and off of the potential helps to keep the particle out of equilibrium. Furthermore, we look at the application of these ratchet devices: the molecular machine, the motor protein. We saw how the activities in the cell are just a typification of the ratchet system.

In chapter two, we looked at the theoretical background of quantum ratchet especially the Hamiltonian quantum ratchet which is the scope of our work. We carefully showed the proof or steps of moving from the dimensional form of the time-dependent Schrodinger equation of our system to its dimensionless form by scaling some variables.

In the third chapter of this work, we discussed the split operator fast Fourier transform, the numerical approach we used in solving our time-dependent Schrodinger equation. In this method, we evolution operator which has the Hamiltonian is split into two parts, the kinetic energy, and the potential energy part. The first half potential energy part acts directly via multiplication on the wave function in the position space. The result is fast Fourier transformed into the momentum space where the kinetic energy part becomes local and acts directly through multiplication. This is then also inverse fast Fourier transformed back into the position space where the second half of the potential energy part acts on it. This

happens in one delta t. The process repeats itself for N times delta t times which is equal to the total time, t required.

After discussing our method, it became easy to compute the time evolution of some observables like momentum (current) and energy and plot their corresponding graphs. We also plotted the momentum distribution curves already in the literature showing that our codes were working correctly. As already seen in the literature, for an initial homogeneous wave function with zero-momentum state and weak potential strength, we found that there is directed current for $\tilde{\hbar}$ with values of half-integer multiple of pi. This type of directed current is caused by resonance. We were able to also show that the energy of such a system with directed current is quadratic. For values of $\tilde{\hbar}$ outside resonance, we saw that the momentum averages to zero for a long time. The momentum distribution curve was handy. We were able to deduce a case of directed transport whereby our momentum distribution curve is asymmetric. On the other hand, in cases of no directed transport, the curve is symmetric.

In chapter four we looked at the implementation of the amplitude noise into our system. Doing this, we were able to get some interesting results. We saw the importance of noise on the current rate for a quantum particle in a flashing asymmetric potential at quantum resonance. First, it helps to enhance the current rate. This is a case where we had a rather weak potential, $P = 0.5$. On the other hand, it is found that for a stronger potential strength at quantum resonance, the presence of noise suppresses the current rate and for the case with the original negative current value, the noise helps in reversing the current to the positive direction, (i.e. current reversal). And lastly, we compared and contrasted the momentum distribution graph for a case of weak potential strength at two noise levels: first, for no noise (minimum current rate) and second, a case with an amount of noise that corresponds to the maximum current rate.

## BIBLIOGRAPHY


[1] R.P. Feynman, R.B. Leighton, and M. Sands, *The Feynman Lectures on Physics, Vol. 1*. Reading, MA: Addison-Wesley. (chapter 46) (1963).

[2] L. Brillouin, Can the rectifier become a thermodynamical demon? *Phys. Rev.*, **78**, 627 (1950).

[3] K. Huang, *Statistical Mechanics*. New York: Ed. Wiley (1987).

[4] C.T.J. Alkemade, On the problem of Brownian motion of non-linear systems. *Physica*, **24**, 1029–1034 (1958)

[5] N. W. Ashcroft, and N. D.Mermin, *Solid State Physics*. Orlando: Saunders College Publishing (1976).

[6] M.V. Smoluchowski, Experimentell nachweisbare, der ublichen Thermodynamik widersprechende Molekularphanomene. *Physik. Zeitschr.*, **13**, 1069 (1912).

[7] A. Ajdari and J. Prost, Mouvement induit par un potentiel p´eriodique de basse symm´etrie: di´electrophor`ese puls´ee. *C. R. Acad. Sci. Paris S´er. II*, **315**, 1635 (1992).

[8] M.O. Magnasco, Forced thermal ratchets. *Phys. Rev. Lett.*, **71**, 1477 (1993).

[9] R. D. Astumian and I. Derenyi, Fluctuation driven transport and models of molecular motors and pumps. *Eur. Biophys. J.*, **27**, 474–489 (1998).

[10] D. Cubero and F.Renzoni, Brownian Ratchets From Statistical Physics to Bio and Nano-motors, Cambridge University Press, (2016).

[11] T. S. Monteiro, P. A. Dando, N. A. C. Hutchings, and M. R.Isherwood, Phys. Rev. Lett. **89**, 194102 (2002).

[12] Anatole Kenfack, Jiangbin Gong, and Arjendu K. Pattanayak, Phys. Rev. Lett. 100, 044104 (2008)

[13] C. Ryu *et al.*, Phys. Rev. Lett. **96**, 160403 (2006).

[14] M. Sadgrove*et al.*, Phys. Rev. Lett. **99**, 043002 (2007);

I. Dana *et al.*, Phys. Rev. Lett. **100**, 024103 (2008).

[15] F. M. Izrailev and D. L. Shepelyanskii, Theor. Math. Phys.**43**, 553 (1980).

[16] A. J. Daley and A. S. Parkins, Phys. Rev. E **66**, 056210 (2002).

[17] F. L. Moore *et al.*, Phys. Rev. Lett. **75**, 4598 (1995).

[18] G. Duffy *et al.*, Phys. Rev. E **70**, 056206 (2004).

[19] E. Lundh and M. Wallin, Phys. Rev. Lett. **94**, 110603 (2005).

[20] D. Poletti, G. C. Carlo, and B. Li, Phys. Rev. E **75**, 011102 (2007).

[21] J. F. Kanem*et al.*, Phys. Rev. Lett. **98**, 083004 (2007).

[22] D. J. Tannor, Introduction to Quantum Mechanics: A Time-Dependent Approach, Chapter 11, University Science Books, (2007).

[23] F. Grossmann, Theoretical Femtosecond Physics: Atoms and Molecules in Strong Laser Field, 2nd edition, Springer, (2013).

[24] A. Vibok, G.G. Balint-Kurti, J. Phys. Chem. **96**, 8712 (1992)

[25] V. Milner, D. A. Steck, W. H. Oskay and M. G. Raizen, Phys. Rev. E 61, 7223 (2000).